Electrohydrodynamic surface instabilities: Role of porous lining at the ablative surface of laser-driven inertial fusion energy target

N. Rudraiah[1,*] and M. Kalal[2]

[1]National Research Institute for Applied Mathematics, 492/G, 7th Cross, 7th Block (West), Jayanagar, Bangalore 560 070, India and UGC-Centre for Advanced Studies in Fluid Mechanics, Department of Mathematics, Bangalore University, Bangalore 560 001, India
[2]Faculty of Nuclear Sciences and Physical Engineering, Czech Technical University in Prague, 11519 Prague 1, Czech Republic

Recent progress in surface instabilities of the Rayleigh–Taylor type at the ablative surface of laser-driven inertial fusion energy (IFE) target is reviewed with the objective of increasing the efficiency of IFE by reducing the growth rate of Rayleigh–Taylor Instability (RTI) using the following two mechanisms: (i) porous lining in the absence of electric force at the ablative surface of the IFE target, i.e. hydrodynamics and magnetohydrodynamics and (ii) porous lining of smart materials of nanostructure in the presence of electric force at the ablative surface of the IFE target, i.e. electrohydrodynamics. The former mechanism deals with two cases. Case 1 is the study of linear and nonlinear RTIs in an ordinary viscous fluid past a densely packed porous lining considering combined lubrication and Stokes approximations. Case 2 deals with RTI considering only Stokes approximation. Mechanism (ii) deals with RTI in a poorly conducting fluid in the presence of a transverse electric field called electrohydrodynamic RTI (ERTI). In both cases a simple theory based on replacing the no-slip condition with Saffman condition with and without thermal radiation is proposed. Both analytical and numerical techniques are used to study RTI. It is shown in both mechanisms, that the porous lining reduces the ratio of growth rates by about 80% compared to about 45% predicted in the literature, over the value that it would have if the target shell is bounded by an impermeable boundary. This finding is useful in the effective extraction of IFE by reducing the asymmetry caused by laser radiation in fusing deuterium–tritium in the target. These mechanisms are also useful in biomedical engineering problems in controlling the effects of plaques in coronary artery diseases and in trachea (i.e. wind pipe in the body).

Keywords: Electrohydrodynamics, inertial fusion energy, porous lining, surface instability.

THE depletion of fossil fuels and atmospheric vagaries have given rise to tremendous strain in providing the required uninterrupted energy supply for the overall development of a country. The crux of the problem in this regard is to find new unconventional sources of energy that are affordable, practical and provide uninterrupted supply of energy which do not have as great an adverse impact on the environment as do fossil fuels. It has been realized[1] that among the many unconventional methods of power generation, one of the effective, efficient and everlasting sources is the inertial fusion energy (IFE). The fuel used in IFE is usually deuterium–tritium (DT), the two isotopes of hydrogen, because they are easily available abundantly in nature, environment-friendly and everlasting sources of energy. One of the important problems faced in the design of IFE target is the loss of symmetry of the target caused by laser radiation in the process of fusing DT to overcome the forces of repulsion between D and T. For efficient extraction of IFE, it is essential to reduce the asymmetry of the target by reducing the growth rate of surface instability at the laser-accelerated ablated surface of the IFE target. Reduction in the growth rate of the surface instabilities represents a field of fundamental research having myriad applications in structural, and biomedical engineering, stellar physics and inkjet printing in addition to IFE. For example, in coronary artery diseases, to remove plaques formed on the walls of the arteries (i.e. endothelium) due to accumulation of cholesterol and other fatty substances and also to remove plaques formed on the walls of the wind pipe (i.e. trachea) due to deposit of unsolvable tiny aerosols, laser radiation is used. This laser intensity erodes the walls causing side effects due to surface instabilities. To reduce the side effects in IFE and in biomedical engineering problems, it is essential to control surface instability. The following three different types of surface instabilities are observed:

(i) Rayleigh–Taylor Instability (RTI), which occurs at an interface between dense fluid and less dense fluid when the latter is at high pressure.
(ii) Kelvin–Helmholtz Instability (KHI), which occurs at an interface subjected to shear.
(iii) Richtmyer–Meshkov Instability (RMI), which occurs due to shock-accelerated interface and is regarded as a special case of RTI.

*For correspondence. (e-mail: rudraiahn@hotmail.com)

In the present review we concentrate only on RTI, which is one of the physical mechanisms limiting the performance of laser fusion targets and hence additional mitigation of RTI growth rate is needed in order to achieve high gain in IFE target by reducing the side effects caused by laser radiation in IFE and in biomedical problems explained above.

At present the following mechanisms are used to reduce the RTI growth rate:

(i) Gradual variation of density assuming plasma as an incompressible heterogeneous fluid in the absence of surface tension.
(ii) Considering compression of DT caused by laser radiation without surface tension.
(iii) IFE target shell with foam layer.
(iv) Ablation surface lined with porous lining of nanostructured smart material.

Numerous numerical and experimental data on RTI growth rate at the ablative surface fit the formula (see Rudraiah *et al.*[2])

$$n = A\sqrt{\ell g/(1+\varepsilon \ell L)} - \beta \ell v_a, \tag{1}$$

where n is the growth rate, ℓ the wavenumber of the perturbation, g the acceleration due to gravity at the interface, ε a constant multiplying the density gradient correction term, L the density scale length at the ablation surface, A the Atwood's number, β a constant multiplying the ablation stabilization, and v_a the flow velocity across the ablation front. The first term on right hand side of eq. (1) is the growth rate n_b, for the classical RTI, namely an incompressible inviscid fluid in the absence of any additional mechanism to reduce the growth rate; the second term is the effect of considering a mechanism to reduce the growth rate. The values of A, ε and β provided by various authors fit eq. (1) are given in Table 1.

At present the available work on the use of foam and variation of density to reduce the RTI growth rate pertain to experimental work and no simple theoretical formula similar to eq. (1) is available. Recently, Rudraiah[3] found an analytical expression analogous to eq. (1) using nanostructured smart porous lining at the ablative surface made of foametal or aloxite[4], of the form

$$n = n_b - \beta \ell v_a, \tag{2}$$

where $n_b = \frac{1}{3}\ell^2(1-(\ell^2/B))$, $B = \delta h^2/\gamma$ is the Bond number, $\delta = g(\rho_p - \rho_f)$ and γ the surface tension. $\beta = (3\alpha\sigma/(4 + \alpha\sigma))$ and $v_a = (4 + \alpha\sigma)/(12(1 + \alpha\sigma))\ell(1 - (\ell^2/B))$ is the velocity of the ablation front. The other quantities have the same meaning as in eq. (1). The first term on right hand side of eq. (2) is the classical growth rate in the absence of nanostructured porous lining and in the presence of surface tension, which is the same as the one given by Babchin *et al.*[5]. The maximum growth rate n_m, for maximum wavenumber, $l_m = \sqrt{B/2}$ is

$$n_m = \frac{B(4+\alpha\sigma)}{48(1+\alpha\sigma)}. \tag{3}$$

Data obtained from eq. (3) are also listed in Table 1.

In IFE, ablatively laser-accelerated surface induces RTI both in acceleration and deceleration phases, which destroys the symmetry of the imploding target and reduces the efficiency of extraction of IFE[6,7].

In this review we discuss the following problems with the objective of reducing the asymmetry of IFE target caused by RTI.

(i) Linear and nonlinear RTI in an incompressible viscous fluid in a channel bounded on one side by rigid boundary and on the other side by a porous layer, considering combined lubrication and Stokes approximations (i.e. unidirectional flow). Linear RTI will be called Problem 1 and nonlinear RTI as Problem 2.
(ii) Linear RTI with the same geometry given in problem 1 considering only Stokes with lubrication approximation, that is, two-dimensional flow. This will be denoted as Problem 3.
(iii) Effects of laser radiation and porous lining on RTI in an ablatively accelerated plasma. This will be denoted as Problem 4.
(iv) Effects of magnetic field, laser radiation, nanostructured porous lining on RTI in an ablative laser accelerated plasma. This will be called Problem 5.
(v) ERTI in thin IFE target lined with smart materials of nanostructure porous lining in the presence of transverse electric field. This will be called Problem 6.

The results obtained are of immense use in some biomedical engineering problems as discussed earlier.

Table 1. Ratio of maximum growth rate

Author	A	ε	β	n_m/n_{bm}
Takabe *et al.*[12]	0.90	0.0	3.00	0.45 n_{bn}
Lindl *et al.*[27]	1.00	1.0	3.00	Silent
Betti *et al.*[28]	0.98	1.0	1.70	Silent
Kilkenny *et al.*[29]	0.90	1.0	3.00	Silent
Knauer *et al.*[30]	0.90	1.0	3.02	Silent
Rudraiah[3]	1.00	1.0	0.75	0.79 n_{bm} ($\alpha = 0.1$, $\sigma = 4$)
			2.86	0.26 n_{bm} ($\alpha = 4$, $\sigma = 20$)

Objective of this review and a brief literature survey

At present as stated earlier, mechanisms like gradual variation of density instead of abrupt change at the abla-

tion interface, compression in a non-viscous fluid and target shell with porous foam have been generally used in the literature (see Table 1) to reduce the growth rate of RTI.

The work of Desai and Pant[8] on the reduction of RTI growth rate was based on experiments involving X-ray transport pertaining to the use of plastic foil targets. Borisenko and Merkuiev[9] used viscoelastic forces and the induced magnetic field to reduce the growth rate of RTI. Recently, Mikaelian[10] has studied the effect of surface tension to reduce the growth rate of RTI. Rudraiah *et al.*[11] have considered the combined effects of surface tension, viscosity and magnetic field as additional factors in reducing RTI growth rate during acceleration. The works mentioned above were concerned with incompressible fluid in the absence of heat transfer and radiation mechanisms. However, the study of RTI in a compressible fluid, including heat transfer is sparse. A good estimation of the growth rate of linear RTI in a non-viscous fluid taking into account the compression due to laser without heat transfer has already been reported[12,13].

Takabe *et al.*[12] have expressed the growth rate of RTI in the form

$$n = 0.9\sqrt{\ell g} - \beta \ell v_a, \tag{4}$$

where $\beta \approx 3$–4, v_a is the flow velocity across the ablative front and ℓ the wavenumber. The first term on the right hand side of eq. (4) is the classical growth rate of RTI, i.e. in the absence of compression and the second term is the effect of compression. The result given by eq. (4) is in conformity with the fact that compression reduces the growth rate in comparison with classical growth rate pertaining to incompressibility. Physically, this reduction in the growth rate due to compression of a non-viscous fluid is due to the fact that compression absorbs some of the energy which would otherwise enter into the fluid motion. Apart from the compression effect, during the past one and a half decades, porous IFE-relevant ablation layers made up of foams have been considered by researchers[14,15] to reduce the RTI growth rate. Sethian *et al.*[14] have developed and evaluated experimentally, new type of targets using low density CH foam shell filled with DT, which minimizes the RT growth rate. Recently, Carles *et al.*[16] have used a magnetic field gradient to study RTI both theoretically and experimentally; good agreement was found between the results of theory and experiments. They have concluded that the technique of magnetic levitation promises to broaden significantly the accessible parameter space of gravitational interfacial instability experiments. We note that the foam used as a porous medium in IFE may deform causing contraction and expansion of flow in the pores resulting in turbulent flow[17]. To achieve laminar flow it is advantageous to consider nanostructured, non-deformable porous matrix like foametal for which the permeability $k = (1.1\text{–}2.7) \times 10^{-5}$ sq. in and aloxide with $k \approx (1.0\text{–}2.48) \times 10^{-6}$ sq. in (see the experiments of Beavers and Joseph[4]), and with low porosity (0.016–0.027) where the creeping flow prevails.

In the case of nanostructured porous lining, the voids made up of nanocrystals are small and hence in this review we use densely packed porous matrix layer saturated with dense fluid of density ρ_p lined with IFE target shell to reduce the growth rate of RTI, with the aim to improve the efficiency of extraction of fusion energy. The assumption of incompressibility assumed in our work is adequate since the perturbations considered here are not bounded by gravitational scale height[18], but depends on the surface tension scale of the system. Though these assumptions are severe, our aim is to show that the dense incompressible fluid-saturated porous lining in the absence of heat transfer reduces the growth rate of RTI considerably compared to that in the absence of porous lining. Physically, the porous layer absorbs the energy of the fluid and dampens the system, which is analogous to the compression case discussed by Takabe *et al.*[12]. In spite of the simplicity of the model explained above, much work has not been done using a simple model of densely packed non-deformable incompressible fluid-saturated porous lining to reduce the growth rate of RTI in the IFE target. Therefore, the primary objective of this review is to use a porous lining to suppress the growth rate of RTI modes. In the case of radiation considered in some of the problems, we will deal with Boussinesq fluid.

To achieve the objective, the plan of this review is as follows. The basic equations and the relevant boundary and surface conditions, using suitable approximations[19], are discussed in detail. The velocity distribution and dispersion relation are obtained analytically while dealing with particular problems using linear and nonlinear stability analysis. Important conclusions are drawn in the final section.

Mathematical formulation

We consider a thin target shell in the form of a film of unperturbed thickness h filled with an incompressible, viscous, light fluid of density ρ_f bounded on one side by a rigid surface and on the other side by a dense incompressible viscous fluid-saturated densely packed nanostructure porous lining of large extent compared to the shell thickness h (Figure 1). The assumption regarding density is necessary for RTI and the assumption on porous lining is necessary to maintain laminar flow using the Darcy equation[17] and Saffman[20] slip condition. The fluid in the shell is set in motion by acceleration normal to the interface and small disturbances are amplified when the acceleration is directed from the light fluid in the shell to heavy fluid in the porous lining. This instability at the interface is the RTI as defined earlier. We consider the rectan-

gular coordinate system (x, y) as shown in Figure 1, with x-axis parallel to the shell and y-axis normal to the shell and with $\eta(x, t)$ as the perturbed interface between fluid in the film shell and in a porous lining. We note that the Saffman[20] condition is derived on the assumption of nominal surface[19]. It is defined as a smooth geometrical surface drawn in the fluid such that the outermost perimeters of all surface pores of the permeable material are on this surface. If the surface pores are filled with fluid to the level of the respective perimeters, a smooth boundary would result called nominal surface at $y = h$. We note that since the porous lining is a non-deformable porous matrix, it cannot move and perturbation in the fluid penetrates the porous lining through the pores and produces oscillations. This assumption which is used in the experiments of Beavers and Joseph[19] is needed to use the Saffman[20] slip condition given below.

The basic equations of the film–porous lining composite system, following Rudraiah[17] are the conservation of momentum

$$\bar{\rho}\left(\frac{\partial \vec{q}}{\partial t}+(\vec{q}\cdot\nabla)\vec{q}\right)=-\nabla p+\bar{\mu}_{\mathrm{f}}\nabla^2\vec{q}-K\vec{q}, \tag{5}$$

the conservation of mass for Boussinesq fluid

$$\nabla\cdot\vec{q}=0, \tag{6}$$

the equation of state

$$\rho_{\mathrm{i}}=\rho_0[1-\alpha_{\mathrm{T}}(T_{\mathrm{f}}-T_0)], \tag{7}$$

where $\vec{q}=(u,v)$ is the velocity, T_{f} the temperature of fluid in the shell.

$$\bar{\rho}=\rho_{\mathrm{f}}\left[1+X_{\mathrm{p}}\left(\frac{\rho_{\mathrm{p}}}{\rho_{\mathrm{f}}}-1\right)\right],$$

the density,

$$\bar{\mu}=\mu_{\mathrm{f}}\left[1+X_{\mathrm{p}}\left(\frac{\mu_{\mathrm{ef}}}{\mu_{\mathrm{f}}}-1\right)\right],$$

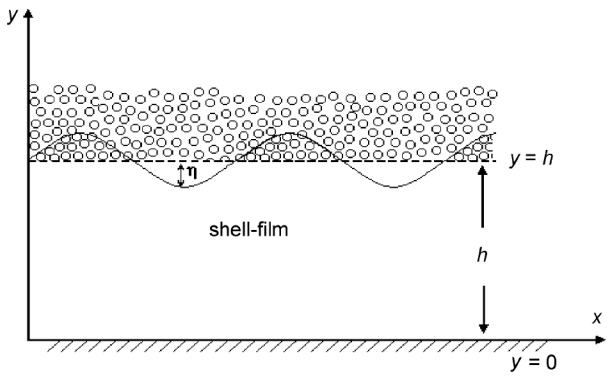

Figure 1. Physical configuration.

the viscosity,

$$K=X_{\mathrm{p}}\left(\frac{\mu_{\mathrm{f}}}{k}+\frac{\rho_{\mathrm{p}}C_{\mathrm{b}}}{\sqrt{k}}|q|\right),$$

and suffixes p and f denote porous lining and fluid film shell respectively, μ_{ef} is the effective (or Brinkmann) viscosity, μ_{f} viscosity of fluid within the shell, k the permeability (which has the dimension of length-squared) of porous lining, C_{b} the drag coefficient and

$$X_{\mathrm{p}}=\begin{cases}0 & \text{for shell}\\ 1 & \text{for porous lining.}\end{cases}$$

These equations have to be supplemented with suitable boundary and interface conditions to be discussed later and the conservation of energy will also be discussed later while dealing with the effect of laser radiation on RTI.

We deal with linear unidirectional and two-dimensional RTI by considering an infinitesimally small disturbance superposed on the basic state and nonlinear RTI is studied numerically using both harmonic evolution of the interface and numerical integration. The basic state is quiescent and the interface is a nominal surface[4]. We note that the two-dimensional analysis is sufficient for drawing conclusions about linear stability analysis because the results can be readily used to predict the behaviour of three-dimensional motion[21]. For example, the three-dimensional disturbances with wavenumbers ℓ and m along the x- and z-directions respectively, have the same stability behaviour as a two-dimensional disturbance with the wavenumber $\alpha_0 = (\ell^2 + m^2)^{1/2}$. Further, to understand the physics of the problems considered in this review, following Babchin *et al.*[5] and Rudraiah *et al.*[19], we restrict our analysis to flows satisfying either the combined Stokes and lubrication approximations[17] or Stokes approximation only[19]. That is (i) $\eta << h$, where η is the elevation of the interface and h the thickness of the film. These assumptions help to neglect the variation of u with respect to x. (ii) The Bond number $B = \delta h^2/\gamma << 1$, which implies gravitational force is negligible compared to surface tension force, where γ is the surface tension and $\delta = g(\rho_{\mathrm{p}} - \rho_{\mathrm{f}})$ is the normal stress. (iii) The Reynolds number $R = Uh^2/L\nu << 1$, which ensures laminar flow and also enables to neglect inertial force. (iv) The Strouhal number S, which is the measure of the ratio of local acceleration (i.e. $\partial\vec{q}/\partial t$) to the inertial acceleration $((\vec{q}\cdot\nabla)\vec{q})$ is small, i.e.

$$S=\frac{L}{t_0U}<<1,\quad L=\sqrt{\left(\frac{\gamma}{\delta}\right)},$$

where t_0 is the characteristic time and U the characteristic velocity which enables to neglect local acceleration in the

momentum equation. Approximations (i)–(iv) are the usual lubrication and Stokes approximations which help to neglect many terms, particularly the non-linear terms in the basic equations (eqs (5) and (6)). We also assume that heavy fluid in a porous lining is almost static because of creeping flow approximation in a densely packed porous medium, which is needed to use Saffman[20] slip condition.

Particular problems in hydrodynamics and magnetohydrodynamics

Problem 1: Effects of porous lining on the reduction of growth rate of RTI in IFE target in hydrodynamics with lubrication and Stokes approximations

In this section, following Rudraiah[3], we consider a porous lining at the ablative surface and obtain the classical RTI (i.e. absence of porous lining) as a particular case when the permeability of the porous lining $k \to \infty$. Under lubrication and Stokes approximations discussed earlier following an analysis of Rudraiah[3], the basic equations (eqs (5) and (6)) reduce to

$$0 = -\frac{\partial p}{\partial x} + \mu_f \frac{\partial^2 u}{\partial y^2}, \quad 0 = \frac{\partial p}{\partial y} \text{ and } \frac{\partial u}{\partial x} + \frac{\partial v}{\partial y} = 0, \qquad (8a\text{–}c)$$

where u and v are the x and y components of velocity of fluid in the film-shell and p the pressure (see Figure 1). These equations have to be solved using the following boundary and surface conditions.

The no-slip condition at the rigid surface is

$$u = v = 0 \quad \text{at } y = 0. \qquad (9)$$

The Saffman[20] slip condition at the porous lining and thin-film interface is

$$\frac{\partial u}{\partial y} = -\frac{\alpha}{\sqrt{k}} u \quad \text{at } y = h, \qquad (10)$$

where α is the slip parameter and k is the permeability.

The dynamic condition at the interface is

$$p = -\delta\eta - \gamma \frac{\partial^2 \eta}{\partial x^2}, \quad \text{at } y = h, \qquad (11)$$

and the kinematic condition at the interface is

$$v = \frac{\partial \eta}{\partial t} + u \frac{\partial \eta}{\partial x} \quad \text{at } y = h, \qquad (12)$$

where η is the elevation of the free surface. For the linear case this kinematic condition reduces to

$$v = \frac{\partial \eta}{\partial t} \quad \text{at } y = h. \qquad (13)$$

Making these equations dimensionless using the scales h for length, δh for pressure, $\delta h^2/\mu_f$ for velocity and $\mu_f/\delta h$ for time and solving them, we get

$$u = \frac{y}{2}\left[y - \frac{(2+\alpha\sigma)}{(1+\alpha\sigma)} \right] \frac{\partial p}{\partial x}, \qquad (14)$$

where $\sigma = h/\sqrt{k}$ is the porous parameter.

Integrating eq. (8c) with respect to y from 0 to 1, using eq. (14) and simplifying, we get

$$v(1) = -\frac{1}{6}\left[1 - \frac{3(2+\alpha\sigma)}{2(1+\alpha\sigma)} \right] \frac{\partial^2 p}{\partial x^2}. \qquad (15)$$

This is analogous to v_a in eq. (1) given by Takabe *et al.*[12] for compression of non-viscous fluid. From eq. (8c), using the normal mode solution of the form $\eta = \eta_0 e^{i\ell x + nt}$ and using eqs (11) and (15), we get the dispersion relation of the form

$$n = \left[\frac{1}{3} - \frac{\alpha\sigma}{4(1+\alpha\sigma)} \right] \ell^2 \left(1 - \frac{\ell^2}{B} \right), \qquad (16)$$

where n is the growth rate and $B = \delta h^2/\gamma$ the Bond number.

In the absence of porous lining ($k \to \infty$, i.e. $\sigma \to 0$), the growth rate (eq. (16)) reduces to

$$n_b = \frac{\ell^2}{3}\left(1 - \frac{\ell^2}{B} \right), \qquad (17)$$

which coincides with the expression given by Babchin *et al.*[5]. Hence,

$$n = n_b - \frac{\alpha\sigma}{4(1+\alpha\sigma)} \ell^2 \left(1 - \frac{\ell^2}{B} \right) = n_b - \beta \ell v_a, \qquad (18)$$

where

$$\beta = \frac{3\alpha\sigma}{(4+\alpha\sigma)} \quad \text{and} \quad v_a = \frac{(4+\alpha\sigma)}{12(1+\alpha\sigma)} \ell \left(1 - \frac{\ell^2}{\beta} \right).$$

The second term on the right hand side of eq. (18) is analogous to the second term in eq. (1) given by Takabe *et al.*[12]. Some important conclusions are drawn later in this review.

Problem 2: Nonlinear evolution of interface in hydrodynamics

In the kinematic condition (eq. (12)) for u, we use the approximation

$$u(\eta) = u(h) + \left.\frac{\partial u}{\partial \eta}\right|_{y=h}^{\eta}.$$

This, using eq. (10), becomes

$$u(\eta) = u(h) - \frac{\alpha}{\sqrt{k}} u(h)\eta = \left(1 - \alpha\sigma\frac{\eta}{h}\right)u(h). \tag{19}$$

Then using eq. (19), eq. (12) becomes

$$v(h) = \frac{\partial \eta}{\partial t} + \left(1 - \alpha\sigma\frac{\eta}{h}\right)u(h)\frac{\partial \eta}{\partial x}. \tag{20}$$

From eq. (8c), we get

$$v(h) = -\int_0^h \frac{\partial u}{\partial x}\,\mathrm{d}y. \tag{21}$$

Solution of eq. (14) in dimensional form is

$$u = \frac{1}{2\mu}\frac{\partial p}{\partial x}\left[y - h\frac{(2+\alpha\sigma)}{(1+\alpha\sigma)}\right]y. \tag{22}$$

Using eqs (11), (21) and (22), eq. (11) becomes

$$\frac{\partial \eta}{\partial t} + \frac{h^2\left(1-\alpha\sigma\frac{\eta}{h}\right)}{2\mu(1+\alpha\sigma)}\left[\delta\frac{\partial \eta}{\partial x} + \gamma\frac{\partial^3 \eta}{\partial x^3}\right]\frac{\partial \eta}{\partial x}$$

$$= \frac{h^3(4+\alpha\sigma)}{12\mu(1+\alpha\sigma)}\left[\delta\frac{\partial^2 \eta}{\partial x^2} + \gamma\frac{\partial^4 \eta}{\partial x^4}\right]. \tag{23}$$

If η is very large, i.e. $\eta >> hs$, then the linear terms in eq. (23) can be neglected and we obtain:

$$\frac{\partial \eta}{\partial t} + \frac{h^2\left(1-\beta\frac{\eta}{h}\right)}{2\mu(1+\beta)}\left[\delta\frac{\partial \eta}{\partial x} + \gamma\frac{\partial^3 \eta}{\partial x^3}\right]\frac{\partial \eta}{\partial x} = 0 \tag{24}$$

where $\beta = \alpha\sigma$.

The process described is quite different from that in which the film is bounded by a fluid layer with moving boundaries instead of a porous layer, as discussed by Babchin *et al.*[5]. Therefore, we use eq. (23) to study nonlinear evolution. Equation (23) is not amenable to analytical treatment and hence we solve it numerically using fourth order central differences in space and time as explained below. For time-integration of eq. (23) Adams–Bashforth predictor and Adams–Moulton corrector steps of fourth order are used, as described in Chapra and Canale[23]. Spatial derivatives are discretized by the following central difference formulae of fourth-order accuracy:

$$\frac{\partial \eta(x)}{\partial x} \mapsto \frac{1}{12\Delta x}[\eta(i-2) - 8\eta(i-1) + 8\eta(i+1) - \eta(i+2)], \tag{25}$$

$$\frac{\partial^2 \eta(x)}{\partial x^2} \mapsto \frac{1}{12\Delta x^2}[-\eta(i-2) + 16\eta(i-1) - 30\eta(i) + 16\eta(i+1) - \eta(i+2)], \tag{26}$$

$$\frac{\partial^3 \eta(x)}{\partial x^3} \mapsto \frac{1}{8\Delta x^2}[-\eta(i-3) - 8\eta(i-2) + 13\eta(i-1) - 13\eta(i+1) + 8\eta(i+2) - \eta(i+3)], \tag{27}$$

and

$$\frac{\partial^4 \eta(x)}{\partial x^4} \mapsto \frac{1}{6\Delta x^4}[-\eta(i-3) + 12\eta(i-2) - 39\eta(i-1) + 56\eta(i) - 39\eta(i+1) + 12\eta(i+2) - \eta(i+3)]. \tag{28}$$

The abbreviated notation, e.g. $\eta(i-2)$, stands for the value of η at the position $x - 2\Delta x$. The integer i indicates the ith grid point.

The initial condition used in the numerical integration is a sine-wave with wavenumber ℓ:

$$\eta(x,0) = \eta_0 \sin(\ell x). \tag{29}$$

The amplitude η_0 is assumed to be small. Its non-dimensional value is $\hat{\eta}_0 = 10^{-4}$.

Periodic boundary conditions have been applied in the x-direction.

In Figures 2 and 3, we present not only linear, but also nonlinear results for two different values of $\hat{h} = h/(\gamma/\delta)^{1/2}$ of the fluid layer, namely $\hat{h} = 0.1$ and 1, and three values of the parameter $\beta = \alpha\sigma$, namely 0.1, 2.0, 100.0, which are the representative values. While the linear results are characterized by curves with the symbols □, ○, △, the nonlinear results are represented by simple curves (solid, dashed and dashed–dotted). In the case of linear results, the vertical axes of Figures 2 and 3 represent the growth rate $\hat{n} = \mu n/\sqrt{\gamma\delta}$ of the interface perturbation $\hat{\eta} = \eta/h$. In the nonlinear case it provides the relative time rate of change of $\hat{\eta}_{\max}$, $(1/\hat{\eta}_{\max})(\partial\hat{\eta}_{\max}/\partial t)$. $\hat{\eta}_{\max}$ denotes the maximum nondimensional perturbation of the interface. It turns out that both the quantities coincide perfectly for thick fluid layers, given by $\hat{h} = 0.1$, i.e. $h = (\gamma/\delta)^{1/2}$ (Figure 3). In other words, if the thickness of the fluid layer is of the order of $(\gamma/\delta)^{1/2}$, the interface evolves linearly. On the other hand, thin fluid layers (e.g. $\hat{h} = 0.1$, Figure 2) are more sensitive to buoyancy and/or surface tension effects and undergo a nonlinear temporal evolution, irre-

spective of the wavenumber $\hat{\ell} = \lambda \ell$, $\lambda = \sqrt{\gamma/\delta}$. Again $\hat{\ell} = 1$ represents a special case. We also conclude from Figures 2 and 3 that the shape of the dispersion curves in the linear and nonlinear cases is controlled by the porous parameter β alone. There are no qualitative differences between 'thick' and 'thin' fluid layers. When h becomes very large, however, the approximations mentioned earlier make the linear and nonlinear results coincide.

Finally, it is interesting to discuss the spatial structure of the relative growth rate of the interface in terms of the quantity

$$n_{\mathrm{NL}} - n_{\mathrm{NL,max}} = \frac{1}{\hat{\eta}} \frac{\partial \hat{\eta}}{\partial \hat{t}} - \frac{1}{\hat{\eta}_{\max}} \frac{\partial \hat{\eta}_{\max}}{\partial \hat{t}}$$

at an early stage, before instability occurs for two wavenumbers $\hat{\ell} = 0.75$ and 2.0, and the three porous parameters β selected in Figures 2 and 3. In fact, the instant of time considered in these thin layers results in $\hat{\ell} = 5 \times 10^{-4}$, which is close to the initial time. We found six waves in the interval 16π. The peaks exist and reflect the positions of the wave modes. Since $n_{\mathrm{NL,max}} = 0$ for $\beta = 100$, the peaks are the positions where the growth rate is maximum. This is not true for $\beta = 0.1$ and 2.0, where the positions for $n_{\mathrm{NL,max}}$ coincide with those of the wave crests. In the case of large wavenumbers, 16 complete waves are stored in the interval 16π. Compared to the $\hat{\ell} = 0.75$ case the amplitudes have increased, but the shapes of the interface growth rates are qualitatively the same. We found that full numerical solutions deviate from a simple harmonic behaviour of η, namely $\eta(x, t) = \eta_0(t)\sin(\ell x)$ and the general solutions were close to the simple harmonic waves for the long interval considered. Computations at the later times became unstable. The presumed solution deviates earlier from the general solution when the wavenumber is small (for details see Rudraiah *et al.*[24]).

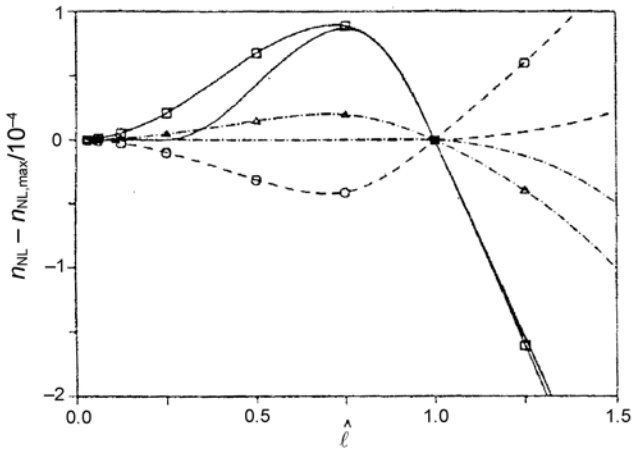

Figure 2. Linear (curves with symbols) and nonlinear (simple curves) dispersion relations for three different values of β ($\beta = 0.1$: ---; $\beta = 2.0$; ——; $\beta = 100.0$: –·–·–) and a thin fluid layer of thickness, $h = 0.1(\gamma/\delta)^{1/2}$.

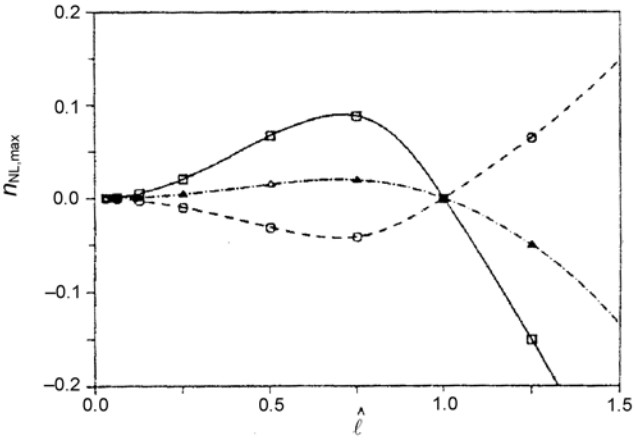

Figure 3. Linear and nonlinear dispersion relations for three different values of β ($\beta = 0.1$: ---; $\beta = 2.0$; ——; $\beta = 100$: –·–·–) and thick fluid layer with $h = (\gamma/\delta)^{1/2}$.

Problem 3: Two-dimensional linear evolution of interface using only Stokes approximation in hydrodynamics

Using the approximations discussed earlier, except the Stokes approximations[24], namely $h/L << 1$, eqs (5) and (6) as $k \to \infty$, for two-dimensional flow, take the form

$$\frac{\partial^2 u}{\partial x^2} + \frac{\partial^2 u}{\partial y^2} = \frac{1}{\mu_{\mathrm{f}}} \frac{\partial p}{\partial x}, \quad \frac{\partial^2 v}{\partial x^2} + \frac{\partial^2 v}{\partial y^2} = \frac{1}{\mu_{\mathrm{f}}} \frac{\partial p}{\partial y} \quad \text{and}$$

$$\frac{\partial u}{\partial x} + \frac{\partial v}{\partial y} = 0. \qquad (30a\text{–}c)$$

The required boundary and interfacial conditions are given by eqs (11)–(14) replacing eq. (12) by the condition

$$\frac{\partial u}{\partial x} + \frac{\partial v}{\partial y} = -\frac{\alpha}{\sqrt{k}} u. \qquad (31)$$

The question of interest here is to determine the growth rate for a small periodic perturbation of the interface. For this we look for the solution of the form

$$(u, v, \eta) = \{u(y), v(y), \eta(y)\} \exp(nt + \mathrm{i}\ell x). \qquad (32)$$

Substituting eq. (32) into eqs (30) and (31), and simplifying[24], we get

$$D^4 v - 2\ell^2 D^2 v + \ell^4 v = 0, \qquad (33)$$

where $D = \mathrm{d}/\mathrm{d}y$. This has to satisfy the following conditions:

$$v = Dv = 0 \quad \text{at } y = 0,$$

$$(D^2 + \ell^2) v = \frac{\alpha}{\sqrt{k}} Dv \quad \text{at } y = h,$$

$$p = \frac{\mu}{\ell^2}(D^3 v - \ell^2 Dv) \quad \text{at } y = h \text{ and } \tilde{v}(h) = m\tilde{\eta}. \quad \text{(34a–d)}$$

Following the same procedure in deriving eq. (18), we get

$$\hat{n} = (1-\hat{\ell}^2)\frac{\hat{N}}{\hat{\ell}}, \quad (35)$$

where

$$\hat{N} = \frac{\dot{S}\dot{C} - \ell h + \beta(2\ell h)^{-1}(\ell^2 h^2 - \dot{S}^2)}{2\dot{C}^2 + \ell^2 h^2 - \beta(1+\dot{S}\dot{C})},$$

$$\hat{n} = \frac{\mu n}{\sqrt{\gamma\delta}}, \quad \hat{\ell} = \lambda\ell, \quad \lambda = \sqrt{\frac{\gamma}{\delta}}$$

and $\dot{C} = \cosh(\ell h)$, $\dot{S} = \sinh(\ell h)$, $\beta = \alpha\sigma$. (36)

In the limit $\beta \to 0$, $N \to N_0$, where

$$N_0 = \frac{\dot{S}\dot{C} - \ell h}{2\dot{C}^2 + \ell^2 h^2}, \quad n_b = \frac{(\delta - \gamma\ell^2)N_0}{\mu\ell}. \quad (37)$$

Problem 4: Effects of laser radiation and porous lining on RTI in an ablatively laser-accelerated fluid in hydrodynamics

In this case, in addition to the conservation of momentum given by eq. (5), conservation of mass given by eq. (6) and equation of state given by eq. (7), we need the conservation of energy with radiation given by

$$(X_p(M-1)+1)\frac{\partial T}{\partial t} + (\vec{q}\cdot\nabla)T = (X_p(\kappa'-1)+1)\nabla^2 T \pm I_0\Omega e^{-\Omega y}, \quad (38)$$

where the temperature $T = T_p$ for porous layer, $T = T_f$ for fluid in the film, and $T = T_0$ for rigid surface. $\kappa' = \kappa_{ef}/\kappa$, where κ is the thermal diffusivity of the fluid, κ_{ef} the effective thermal diffusivity in the presence of porous layer. Ω is the absorption coefficient, $M = (\rho c_p)_p/(\rho c_p)_f$ the heat capacity ratio. All other quantities have the same meaning as in eqs (5) and (6) and (±) in the last term of eq. (38) will depend on the physical situation, namely whether energy is gained or lost.

We use the conditions given by eqs (11)–(15) and following the same procedure in obtaining eq. (18) and using

$$\delta = g(\rho_p - \rho_f), \quad \rho_p = \rho_0[1-\alpha_T(T_p - T_0)],$$

$$\rho_f = \rho_0[1-\alpha_T(T_f - T_0)],$$

we get

$$n = \left[\frac{1}{3} - \frac{\alpha\sigma}{4(1+\alpha\sigma)}\right]\ell^2\left(\delta(1) - \frac{\ell^2}{B}\right), \quad (39)$$

where $\delta(1) = \theta_{f_1} - \theta_{p_1}$, $\theta = \frac{(T-T_0)}{(T_1-T_0)}$, θ_f for $T = T_f$ and θ_p for $T = T_p$, n is the growth rate and $B = \delta h^2/\gamma$ the Bond number, θ_{p_1} and θ_{f_1} are the values of θ_p and θ_f at $y = 1$. Suffixes f and p refer to fluid and porous lining.

Substituting for $\delta(1)$ in eq. (39) and simplifying, we get

$$n = \frac{(4+\alpha\sigma)}{12(1+\alpha\sigma)}\ell^2\left(\theta_{f_1} - \theta_{p_1} - \frac{\ell^2}{B}\right). \quad (40)$$

The expressions for θ_{p_1} and θ_{f_1} will be given later. In the absence of porous lining ($k \to \infty$, i.e. $\sigma \to 0$) the growth rate (eq. (39)) reduces to

$$n_b = \frac{\ell^2}{3}\left(1 - \frac{\ell^2}{B}\right) - \frac{1}{3}(1 + \theta_{f_1} - \theta_{p_1})\ell^2. \quad (41)$$

Then eq. (39) can be rewritten as

$$n = n_b - \beta\ell v_a, \quad (42)$$

where

$$\beta = \frac{3\alpha\sigma}{4+\alpha\sigma}, \quad v_a = \frac{(4+\alpha\sigma)}{12(1+\alpha\sigma)}\ell\left(\theta_{f_1} - \theta_{p_1} - \frac{\ell^2}{B}\right). \quad (43)$$

For the shell-film

$$v_a\frac{\partial T_f}{\partial y} = \kappa_f\frac{\partial^2 T_f}{\partial y^2} + I_0\Omega e^{-\Omega y}. \quad (44)$$

For the porous lining

$$0 = \kappa_p\frac{\partial^2 T_p}{\partial y^2} \pm I_0\Omega e^{-\Omega y}. \quad (45)$$

Case 1: The fluid in the shell-film and porous lining is homogeneous and incompressible, with temperature T_p in the porous lining assumed to be constant, which maybe higher than the fluid temperature.

Case 2: The fluid in the shell-film as well as in porous lining is assumed to satisfy Boussinesq approximation with varying temperature T_p and T_f. Equation (44) in dimensionless form is

$$v_a\frac{\partial\theta}{\partial y} = \frac{1}{R_a}\frac{\partial^2\theta}{\partial y^2} + Ne^{-\Omega_0 y} \quad (46)$$

where $R_a = \delta h^3/\kappa_f\mu_f)$ is the Rayleigh number because δ has the dimensions of $\rho_0\alpha_T g T_0$, $N = I_0\Omega_0\mu_f/\delta T_0$ and v_a is given by eq. (43) with $\theta_{f_1} - \theta_{p_1} = \delta(1)$, that is δ is constant. Equation (46) is solved using the following two sets of boundary conditions.

Set 1: $\theta = 1$ at $y = 0$ and $\theta = \theta_1$ at $y = 1$, (47a)

Set 2: $\theta = 1$ at $y = 0$ and $\dfrac{d\theta}{dy} = -B_i(\theta_b - 1)$ at $y = 1$, (47b)

where $B_i = h_e h/\kappa_f$ is the Biot number, h_e the heat transfer coefficient from porous layer to the film and θ_b the temperature at $y = 1$. The solution of eq. (46), satisfying eq. (47a) is:

$$\theta(y) = a_0 + a_1 e^{by} - \frac{NR_a e^{-\Omega_0 y}}{\Omega_0(\Omega_0 + b)},$$

$$a_0 = \frac{NR_a(e^b - e^{-\Omega_0})}{\Omega_0(\Omega_0 + b)(e^b - 1)} - \frac{1 - \theta_1 e^b}{1 - e^b},$$

$$b = \frac{BR_a}{48}\frac{(4 + \alpha\sigma)}{1 + \alpha\sigma}, \quad (48)$$

$$a_1 = \frac{\theta_1 - 1}{1 - e^b} + \frac{NR_a}{\Omega_0(\Omega_0 + b)} - \frac{1 - e^{-\Omega_0}}{1 - e^b},$$

$$-\left(\frac{\partial\theta}{\partial y}\right)_{y=1} = \frac{NR_a}{(\Omega_0 + b)} e^{-\Omega_0} + ba_1 e^b. \quad (49)$$

The solution of eq. (46) satisfying the boundary conditions of set 2 is

$$\theta(y) = 1 + a_2(1 - e^{by}) + \frac{NR_a(1 - e^{-\Omega_0 y})}{\Omega_0(\Omega_0 + b)}, \quad (50)$$

where

$$a_2 = \frac{NR_a e^{-(\Omega_0 + b)}}{b(\Omega_0 + b)} + \frac{B_i}{b}(\theta_B - 1)e^{-b},$$

$$a_3 = \frac{1}{[1 - B_i(e^{-b} - 1)/b]},$$

$$\theta_B = a_3 \left[1 + \frac{NR_a(1 - e^{-\Omega_0})}{\Omega_0(\Omega_0 + b)} + \left(\frac{NR_a e^{-\Omega_0} - B_i(\Omega_0 + b)}{b(\Omega_0 + b)} \right)(e^{-c} - 1) \right]. \quad (51)$$

Similarly, eqs (44) and (45) in dimensionless form are

$$v_a \frac{\partial\theta_f}{\partial y} = \frac{1}{R_{af}} \frac{\partial^2\theta_f}{\partial y^2} + Ne^{-\Omega_0 y}, \quad (52)$$

$$0 = \frac{\partial^2\theta_p}{\partial y^2} - N_p e^{-\Omega_0 y}, \quad N_p = \frac{I_0\Omega_0 h^3}{\kappa_p T_0}. \quad (53)$$

The boundary conditions on θ_f and θ_p are

$$\theta_p \to 0 \quad \text{at } y \to \infty,$$
$$\kappa_r \frac{\partial\theta_p}{\partial y} = \frac{\partial\theta_f}{\partial y} \quad \text{at } y = 1,$$
$$\kappa_r = \frac{\kappa_p}{\kappa_f} \text{ and } \theta_f = 1 \quad \text{at } y = 0. \quad (54)$$

Then the solutions of eqs (52) and (53) satisfying the above conditions are

$$\theta_f = 1 + \frac{NR_{af}}{\Omega_0(\Omega_0 + b)}(1 - e^{-\Omega_0 y}) - A_4(1 - e^{by}),$$
$$\theta_p = \frac{N_p}{\Omega_0^2} e^{-\Omega_0 y}, \quad (55a, b)$$

where $b = R_{af}v_a$, and v_a is given by eq. (43) and

$$A_4 = \frac{1}{b}\left[\frac{\kappa_r N_p}{\Omega_0} - \frac{NR_a}{(\Omega_0 + b)} \right] e^{-(\Omega_0 + b)}.$$

From eqs (55a, b) we get

$$\theta_p - \theta_f = -1 + A_4(1 - e^b) - \frac{NR_{af}(1 - e^{-\Omega_0})}{\Omega_0(\Omega_0 + b)} + \frac{N_p e^{-\Omega_0}}{\Omega_0^2}. \quad (56)$$

The growth rate n given by eq. (40) is computed for different values of $\theta_p - \theta_f$ (0.1, 1, 10) and for different values of B (0.01, 0.02, 0.04, 0.06). The results are depicted in Figure 4 *a–c*. Conclusions are drawn later in the article.

Problem 5: Effects of magnetic field, laser radiation and porous lining on RTI in an ablatively laser-accelerated plasma in magnetohydrodynamics

In this section, we discuss the effects of magnetic field, laser radiation and porous lining of nanostructure on RTI at an ablative surface of a thin target shell using linear stability analysis. We consider both incompressible homogeneous and compressible Boussinesq electrically conducting fluid bounded below by a rigid surface and above by a porous layer. The growth rate of RTI, including the effect of radiation is derived, which is analogous to the form given by Takabe *et al.*[12] for compressible fluid and that given by Rudraiah[3] for incompressible fluid with porous

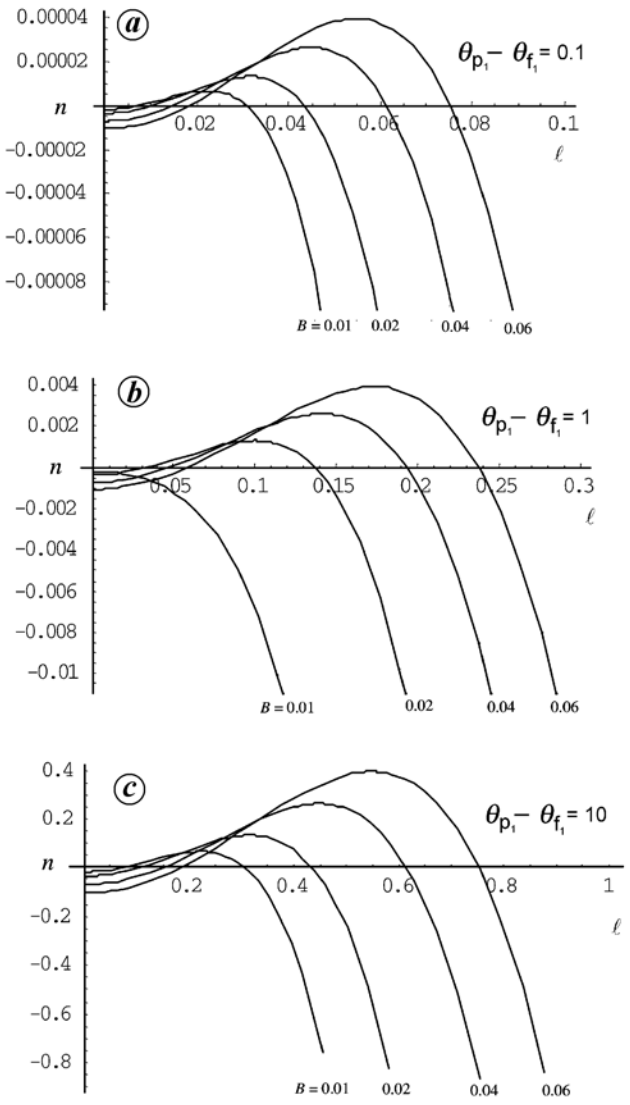

Figure 4 *a–c*. Growth rate vs wavenumber.

lining. It is shown that the magnetic field and porous lining greatly reduce the growth rate. The cut-off and maximum wavenumbers and the corresponding maximum frequency are obtained. The ratio of maximum to classical growth rate is numerically computed and the values are tabulated for different values of the Hartmann number, slip and porous parameters. We found that the combined effect of magnetic field and porous lining reduces the growth rate of RTI considerably compared to the classical growth rate.

Mathematical formulation

The conservation of momentum from eq. (5), by the addition of volume force given by the magnetic field called the Lorentz force $\bar{\mu}_h \vec{J} \times \vec{H}$ is

$$\bar{\rho}\left(\frac{\partial \vec{q}}{\partial t} + (\vec{q}\cdot\nabla)\vec{q}\right) = -\nabla p + \bar{\mu}_f \nabla^2 \vec{q} - K\vec{q} + \bar{\mu}_h \vec{J} \times \vec{H}. \quad (57)$$

The conservation of mass for compressible Boussinesq fluid is the same as eq. (6) with the equation of state

$$\bar{\rho} = \rho_0 [1 - \alpha_T \{ X_p (T_p - T_f) + T_f - T_0 \}]. \quad (58)$$

The conservation of energy is then given by eq. (38). Here, the current density,

$$\vec{J} = \bar{\sigma}_h [\vec{E} + \bar{\mu}_h \vec{q} \times \vec{H}]$$

Maxwell's equations

$$\nabla \cdot \vec{H} = 0, \ \nabla \times \vec{E} = -\mu \frac{\partial \vec{H}}{\partial t}, \quad \nabla \cdot \vec{E} = 0,$$

magnetic permeability,

$$\bar{\mu}_h = \mu_h \left[1 + X_p \left(\frac{\mu_p}{\mu_h} - 1\right)\right]$$

electrical conductivity

$$\bar{\sigma}_h = \sigma_p \left[1 + X_p \left(\frac{\sigma_{hp}}{\sigma_h} - 1\right)\right]$$

and all other quantities are as defined earlier.

Dispersion relation with laser radiation

In this section we derive the dispersion relation as well as temperature distribution incorporating the laser radiation effect. Under the approximations discussed earlier eq. (8a) in the presence of magnetic field becomes

$$0 = -\frac{\partial p}{\partial x} + \frac{\partial^2 u}{\partial y^2} - M^2 u, \quad (59)$$

whose solution satisfying the boundary conditions, eqs (9) and (10) is

$$u = \frac{\left\{\begin{array}{l} M \,\mathrm{ch}[M(1-y)] + \alpha\sigma \,\mathrm{sh}[M(1-y)] \\ + \alpha\sigma[\mathrm{sh}(My) - \mathrm{sh}(M)] - M \,\mathrm{ch}(M) \end{array}\right\}}{[M \,\mathrm{ch}(M) + \alpha\sigma \,\mathrm{sh}(M)]} \times \frac{P}{M^2}, \quad (60)$$

where

$$M = \mu H_0 h \sqrt{\frac{\sigma_h}{\mu_f}}$$

is the Hartman number, σ_h the electric conductivity, $\sigma = h/\sqrt{k}$ the porous parameter, and $\cosh(\theta)$ and $\sinh(\theta)$

are denoted by ch(θ) and sh(θ) respectively. From eq. (8c), using eq. (60) and integrating, and using $v(0) = 0$ at $y = 0$, we get

$$v(1) = \left\{ \frac{\begin{array}{l} 2\alpha\sigma[1-\mathrm{ch}(M)]+(\alpha\sigma-1) \\ \times M\,\mathrm{sh}(M)+M^2\,\mathrm{ch}(M) \end{array}}{M^3[M\,\mathrm{ch}(M)+\alpha\sigma\,\mathrm{sh}(M)]} \right\} \frac{\partial^2 p}{\partial x^2}, \tag{61}$$

Then, following the procedure in deriving eq. (18), we get

$$n = n_b - \beta \ell v_a \tag{62}$$

where n is the growth rate, ℓ is the wavenumber,

$$\beta = \frac{M^3 - 3(M - \mathrm{th}\,M) + \alpha\sigma(M^2-3)\mathrm{th}\,M + \dfrac{6\alpha\sigma(\mathrm{ch}\,M-1)}{M\,\mathrm{ch}\,M}}{3\left[M - \mathrm{th}\,M + \alpha\sigma\,\mathrm{th}\,M + \dfrac{2\alpha\sigma(1-\mathrm{ch}\,M)}{M\,\mathrm{ch}\,M}\right]} \tag{63}$$

is a constant, v_a is the velocity of flow across the ablative front given by

$$v_a = \frac{M - \mathrm{th}\,M + \alpha\sigma\,\mathrm{th}\,M + \dfrac{2\alpha\sigma(1-\mathrm{ch}\,M)}{M\,\mathrm{ch}\,M}}{M^3\left(1+\alpha\sigma\dfrac{\mathrm{th}\,M}{M}\right)} \ell\left(\delta - \frac{\ell^2}{B}\right), \tag{64}$$

th M = tanh M, $B = \delta_0 h^2/\gamma$ is the Bond number, $\delta = 1$ or $(\theta_{f_1} - \theta_{p_1})$, where suffix 1 denotes the values of θ at $y = 1$, and

$$n_b = \frac{\ell^2}{3}\left(\delta - \frac{\ell^2}{B}\right). \tag{65}$$

When $M \to 0$, eq. (62) reduces to eq. (18) and we call it as n_1.

In the absence of porous lining ($k \to \infty$, i.e. $\sigma \to 0$), the growth rate eq. (62) tends to

$$n_2 = n_b - \beta_2 \ell v_{a_2}, \quad \beta_2 = \frac{M^3 - 3(M - \mathrm{th}\,M)}{3(M - \mathrm{th}\,M)},$$

$$v_{a_2} = \frac{(M - \mathrm{th}\,M)\ell(\ell - \ell^2/B)}{M^3}. \tag{66a–c}$$

In the case of using eq. (62) which is $(n_b)_p$, we have

$$n_3 = (n_b)_p - \beta_3 \ell v_{a_3}, \tag{67}$$

where

$$\beta_3 = \frac{\left\{\begin{array}{l} M^3 - 3(M - \mathrm{th}\,M) + \alpha\sigma(M^2-3)\mathrm{th}\,M \\ + \dfrac{6\alpha\sigma(\mathrm{ch}\,M-1)}{M\,\mathrm{ch}\,M} - 3\alpha\sigma M^2(1+\alpha\sigma\,\mathrm{th}\,M) \end{array}\right\}}{3\left[M - \mathrm{th}\,M + \alpha\sigma\,\mathrm{th}\,M + \dfrac{2\alpha\sigma(1-\mathrm{ch}\,M)}{M\,\mathrm{ch}\,M}\right]}$$

and v_{a_3} is the same as eq. (61).

Temperature distribution in the absence of Ohmic dissipation

For the shell-film and for the porous layer, the energy equations are given by eqs (44) and (45).

The selection of a particular sign in eq. (45) will depend on the physical situation. If we choose the positive sign, then θ_p will be negative implying energy will be lost. The problem considered in this article requires the addition of energy to fuse DT. For this we have to choose a negative sign in eq. (45) to ensure positive θ_p. In this section, as earlier, we consider two cases: eq. (46) with v_a given by eq. (45) and the same boundary conditions given by eq. (47a).

Case 1: Homogeneous incompressible fluid: In this case the solution of eq. (46) using eq. (64) and satisfying the conditions, eq. (47a) is

$$\theta(y) = a_0 + a_1 e^{by} - \frac{NR_a e^{-\Omega_0 y}}{\Omega_0(\Omega_0 + b)}$$

$$= 1 + \frac{a_0(e^{by}-1)}{(e^b - 1)} + a_1(1 - e^{-\Omega_0 y}), \tag{68}$$

where

$$a_0 = \theta_1 - 1 - a_1(1 - e^{-\Omega_0}), \quad a_1 = \frac{NR_a}{\Omega_0(\Omega_0 + b)}, \quad b = v_a R_a$$

$$-\left(\frac{\partial\theta}{\partial y}\right)_{y=1} = \frac{NR_a}{(\Omega_0 + b)} e^{-\Omega_0} + b a_1 e^b. \tag{69}$$

Similarly, the solution of eq. (46), satisfying the boundary conditions, eq. (47b) is

$$\theta(y) = 1 + a_2(1 - e^{by}) + \frac{NR_a(1 - e^{-\Omega_0 y})}{\Omega_0(\Omega_0 + b)}, \tag{70}$$

where

$$\theta_B = a_3\left[1 + \frac{NR_a(1 - e^{-\Omega_0})}{\Omega_0(\Omega_0 + b)}\right.$$

$$+\left(\frac{NR_a e^{-\Omega_0} - B_i(\Omega_0 + b)}{b(\Omega_0 + b)}\right)(e^{-b} - 1)\Bigg], \quad (71)$$

$$a_2 = \frac{NR_a e^{-(\Omega_0 + b)}}{b(\Omega_0 + b)} + \frac{B_i}{b}(\theta_B - 1)e^{-b},$$

$$a_3 = \frac{1}{[1 - B_i(e^{-b} - 1)/b]}.$$

Case 2: Boussinesq fluid: The solutions of eqs (52) and (53) using eq. (64) and the boundary conditions

$$\frac{\partial \theta_p}{\partial y} \to 0 \quad \text{as } y \to \infty,\ \theta_f = 1 \quad \text{at } y = 0, \quad (72)$$

$$\frac{\partial \theta_f}{\partial y} = -B_i(\theta_{f_1} - 1), \quad \frac{\partial \theta_p}{\partial y} = -B_i(\theta_{p_1} - 1) \quad \text{at } y = 1, \quad (73)$$

where θ_{f_1} and θ_{p_1} are the values of θ_f and θ_p at $y = 1$, are

$$\theta_f = 1 + a_1(1 - e^{-\Omega_0 y}) + \frac{B_i}{b}(\theta_{f_1} - 1)e^{-b}(1 - e^{by}) + \frac{\Omega_0 a_1}{b}e^{-(\Omega_0 + b)}(1 - e^{by}), \quad (74)$$

and

$$\theta_p = 1 + \frac{N_p}{\Omega_0 B_i}e^{-\Omega_0} + \frac{N_p}{\Omega_0^2}(e^{-\Omega_0} - e^{-\Omega_0 y}). \quad (75)$$

From these we have

$$\delta(1) = \theta_{f_1} - \theta_{p_1} = 1 - a_3 - \frac{N_p}{\Omega_0 B_i}e^{-\Omega_0} - a_3\left[a_1(1 - e^{-\Omega_0}) + \frac{(B_i - \Omega_0 a_1 e^{-\Omega_0})}{b}(1 - e^{-b})\right]. \quad (76)$$

Problem 6: ERTI in thin IFE target lined with smart material of nanostructure porous lining in the presence of transverse electric field

In this section we study ERTI in electrohydrodynamics (EHD) following Rudraiah *et al.*[25]. EHD is the study of the motion of a poorly conducting fluid in the presence of conservative electric field intensity. The electrical conductivity σ, is very small so that induced magnetic field is negligible and there is no applied magnetic field. There will be the effect of both conduction (i.e. dynamic) and convection currents with negligible polarized current.

As pointed out in the earlier sections, the interfacial sciences continues to be the frontier area of research in view of its importance in understanding, control and exploitation of many physical, chemical and biological processes, such as IFE, solidification processes in materials science, biomedical engineering, processes involving friction between surfaces and their mitigation, etc. In IFE, the hollow shells are filled with an equal mixture of D and T fluids at high pressure and then solidified to the cryogenic temperature so that the DT-fluid freezes forming a thin, mushy coating on the inside of the ablative surface of the shell wall. The direct-drive laser heat at this ablative surface causes surface instabilities. The applications cited above, particularly for efficient extraction of IFE, as stated earlier, are required to reduce the growth rate of the surface instability at laser-accelerated ablative surface of IFE target to reduce the asymmetry of the target caused by laser heating. In this section we discuss EHD porous lining concept to reduce growth rate. The physical mechanism involved is explained below.

The physical characteristics of DT are based on a poorly electrically conducting nature, where the electrical conductivity, σ is a strong function of the temperature, or concentration of the mixture of D and T may also be significant in controlling the growth rate of RTI due to the following physical mechanism that prevails in a poorly conducting fluid. The variation of electrical conductivity with temperature produced by laser radiation applied to fuse DT or with concentration arising from the mixture of DT induces free charges not only in the bulk of the fluid in the target but also at the ablative surface. These free charges induce electric field called thermal or concentration electric field. In addition, there may be an applied electric field generated by segmented electrodes that exist at the boundaries of the target. The density of charge distribution ρ_e, interacting with the total (i.e. combined, induced and applied) electric field, $\vec{E}$, produces the current density $\vec{J}$ which acts as sensing and also produces the force $\rho_e\vec{E}$ which acts as actuation. These two properties, namely sensing and actuation, make the material, by definition, a smart material. Further, we consider a material of very low electrical conductivity σ, of the order 10^{-11}–10^{-9} (ohm.m)$^{-1}$ and permeability k of the order 10^{-10}–10^{-9} m^2 which are in the nanoscale range. In other words, the porous lining that we consider here is a nanostructure smart material. This smart material is an alternate to the one made up of piezoelectric material. The mushy layer at the ablative surface by definition is a mixture of solid and fluid phases, and hence can be regarded as a porous lining of nanostructure smart material[22]. That is, we can regard it as a densely packed porous layer. It is of practical importance in IFE to know whether this electric force together with mushy coating may also control RTI growth rate. These aspects have not been given much attention and the study of their effects is the main objective in this section.

To achieve this objective, this section is planned as follows. The mathematical formulation is given below. Here, we mainly deal with very small electrical conductivity, so that we can easily neglect the induced magnetic field. Further, there is no applied magnetic field and hence the Faraday's law of induction reveal that the electric field is conservative. This implies that the electric field can be expressed as the gradient of scalar electric potential ϕ. This potential is determined first using the relevant Maxwell's equations and the continuity of charges together with suitable boundary conditions. Velocity distribution is determined using the modified Navier–Stokes equation, modified in the sense of addition of electric force $\rho_e\vec{E}$ together with Stokes and lubrication approximations and Saffman[20] slip condition. Different types of ERTI problems with or without radiation are investigated. The dispersion relation is obtained using the dynamic and kinematic conditions at the ablative surface. The cut-off and maximum wavenumbers and the corresponding maximum growth rate are obtained and some important conclusions are drawn.

Mathematical formulation: Consider a thin target shell in the form of a film of unperturbed thickness h (region 1) filled with an incompressible, viscous, poorly electrically conducting light fluid of density ρ_f bounded below by a rigid surface at $y = 0$ and above by an incompressible, viscous, poorly conducting heavy fluid saturated in a dense, nanostructured, porous lining whose thickness is large compared to the shell thickness h, of density ρ_p. The fluid in the thin film is set in motion by an acceleration normal to the interface, whereas in the porous lining it is assumed to be uniform and small perturbations amplify the interface when acceleration is directed from the lighter fluid in the thin film to the heavier fluid in the porous lining. This instability at the interface is known as RTI. To investigate RTI, we consider a rectangular coordinate system (x, y) (see Figure 5) with the x-axis parallel to the film and y-axis normal to it. $\eta(x, t)$ is the perturbed interface and is along the y-direction. There are embedded electrodes at the rigid boundary at $y = 0$ and at the nominal surface at $y = h$.

The basic equations of the film–porous lining composite system are as follows:

The conservation of mass for an incompressible fluid is given by eq. (6). The conservation of momentum is given by eq. (5) with the addition of electric force $\rho_e\vec{E}$, i.e.

$$\rho\left(\frac{\partial\vec{q}}{\partial t}+(\vec{q}\cdot\nabla)\vec{q}\right)=-\nabla p+\mu\nabla^2\vec{q}+\rho_e E. \tag{77}$$

The conservation of electric charge is

$$\frac{\partial\rho_e}{\partial t}+\nabla\cdot\vec{J}=0, \tag{78}$$

where $\vec{J}=\sigma\vec{E}+\rho_e\vec{q}$. The first term on the right hand side is conduction (i.e. dynamic) current and the second term is convective current. Substituting $\vec{J}$ into eq. (78), we get

$$\frac{\partial\rho_e}{\partial t}+(\vec{q}\cdot\nabla)\rho_e+\sigma\nabla\cdot\vec{E}+(\vec{E}\cdot\nabla)\sigma=0,$$

$$\sigma=\sigma_0[1+\alpha_h(C-C_0)], \tag{79a, b}$$

where α_h is the volumetric coefficient expansion of conductivity σ. The Maxwell's equations are

$$\nabla\cdot\vec{E}=\frac{\rho_e}{\varepsilon_e},\ \nabla\times\vec{E}=0,\ \text{which implies}\ \vec{E}=-\nabla\phi, \tag{80a, b}$$

where ϕ is the electric potential. Since the electrical conductivity σ varies with concentration C of DT as in eq. (81) below, with negligible advection of concentration, we have

$$\frac{\mathrm{d}^2C}{\mathrm{d}y^2}=0 \quad \text{with } C = C_0 \text{ at } y = 0 \text{ and } C = C_1 \text{ at } y = h. \tag{81}$$

Solving eq. (81) using the given conditions and substituting this solution in eq. (79b), we get

$$\sigma=\sigma_0\left(1+\alpha\frac{y}{h}\right)\approx\sigma_0 e^{\alpha y}, \tag{82}$$

where $\alpha = \alpha_h\beta_1 << 1$, $\beta_1 = \Delta C = C_1 - C_0$, σ_0 is the conductivity at $c = c_0$.

In solving eqs (77) and (79a) following Rudraiah *et al.*[19], we make use of the following EHD approximations:

(i) The electrical conductivity of the liquid σ, is negligibly small, i.e. $\sigma << 1$.

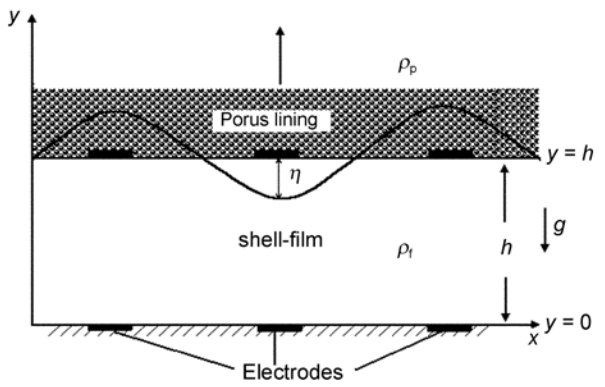

Figure 5. Physical configuration.

(ii) The film thickness h is much smaller than the thickness H of the dense fluid above the film. That is $h << H$.

(iii) The surface elevation η is assumed to be small compared to film thickness h. That is $\eta << h$.

(iv) The Strauhal number S, a measure of the local acceleration to inertial acceleration in eq. (78) is negligibly small. That is $S = L/t_0U << 1$, where the quantities are as defined earlier.

These approximations are usually called Stokes and lubrication approximations, which help to neglect many terms, particularly the nonlinear terms in the basic equations. We also assume that the heavy fluid in the porous lining is almost static because of creeping flow approximation in a densely packed porous medium, which is needed to use the Saffman[20] slip condition.

Under the approximations discussed above the basic equations, i.e. eqs (6) and (77) for fluid in the film reduce to

$$0 = \frac{\partial u}{\partial x} + \frac{\partial v}{\partial y}, \quad 0 = -\frac{\partial p}{\partial x} + \mu \frac{\partial^2 u}{\partial y^2} + \rho_e E_x,$$

$$0 = -\frac{\partial p}{\partial y} + \rho_e E_y. \tag{83a–c}$$

Making eqs (83a–c) dimensionless using

$$u^* = \frac{u}{\delta_1}, \; v^* = \frac{v}{\delta_1}\delta_1 = \frac{\delta h^2}{\mu_f}, \; p^* = \frac{p}{\delta h},$$

$$\rho_e^* = \frac{\rho_e h^2}{\varepsilon_e v_0}, \quad E^* = \frac{v_0}{h}, \; y^* = \frac{y}{h}, \tag{84}$$

and for simplicity neglecting asterisks (*), we get

$$0 = \frac{\partial u}{\partial x} + \frac{\partial v}{\partial y}, \quad 0 = -\frac{\partial p}{\partial x} + \frac{\partial^2 u}{\partial y^2} + We\rho_e E_x,$$

$$0 = -\frac{\partial p}{\partial y} + We\rho_e E_y, \tag{85a–c}$$

where $We = \varepsilon_0 v_0^2 / \delta_0 h^3$ is the electric parameter.

Solution for electric potential ϕ: From eq. (79a) using eq. (80a, b), we get

$$\sigma \frac{\partial^2 \phi}{\partial y^2} + \frac{\partial \phi}{\partial y}\frac{\partial \sigma}{\partial y} = 0. \tag{86}$$

This using eq. (82), becomes

$$\frac{\partial^2 \phi}{\partial x^2} + \frac{\partial^2 \phi}{\partial y^2} + \alpha \frac{\partial \phi}{\partial y} = 0. \tag{87}$$

This equation has to be solved subject to the boundary conditions

$$\phi = x \text{ at } y = 0 \quad \text{and} \quad \phi = x - x_0 \text{ at } y = 1. \tag{88a, b}$$

The nature of these boundary conditions permits a linear variation of ϕ with x. Then the solution of eq. (87), using the above boundary conditions, eq. (88a, b) is

$$\phi = x - \frac{x_0}{1 - e^{-\alpha}}(1 - e^{-\alpha y}). \tag{89}$$

Using eq. (89), eq. (80a) becomes

$$\rho_e = \frac{x_0 \alpha^2}{1 - e^{-\alpha}} e^{-\alpha y},$$

so that

$$\rho_e E_x = -\rho_e \frac{\partial \phi}{\partial x} = \frac{\alpha^2 e^{-\alpha y}}{(1 - e^{-\alpha})}. \tag{90}$$

Dispersion relation: To find the dispersion relation, we have to find the velocity distribution from eq. (85b) using the dimensionless form of boundary and surface conditions given by eqs (9) and (10), with dynamic condition, eq. (11) in the presence of electric field takes the form

$$p = -(1 \pm We)\eta - \frac{1}{B}\frac{\partial^2 \eta}{\partial x^2} \quad \text{at } y = 1, \tag{91}$$

where ± in the first term on the right hand side will depend on whether the applied voltage is along or opposing the gravity.

The solution of eq. (85b), using eqs (9), (10) and (90) in dimensionless form is

$$u = P\frac{y^2}{2} - We a_0 \frac{e^{-\alpha y}}{\alpha^2} + a_1 y + a_2, \tag{92}$$

where

$$P = \frac{\partial p}{\partial x}, \quad a_0 = \frac{\alpha^2}{1 - e^{-\alpha}},$$

$$a_1 = -\left[P\left(\frac{\alpha_p \sigma_p + 2}{2(\alpha_p \sigma_p + 1)} \right) - \frac{We a_0}{\alpha^2 (\alpha_p \sigma_p + 1)} \times (e^{-\alpha} + \alpha e^{-\alpha} - \alpha_p \sigma_p) \right],$$

$$a_2 = \frac{We a_0}{\alpha^2}.$$

In dimensionless form, the kinematic condition eq. (13), takes the form

$$v = \frac{\partial \eta}{\partial t} \quad \text{at } y = 1. \tag{93}$$

From the continuity eq. (83a) and after integrating it using eq. (92), we get

$$v(1) = v_1 = -\int_0^1 \frac{\partial u}{\partial x}\,dy = \left(\frac{4+\alpha_p\sigma_p}{12(1+\alpha_p\sigma_p)}\right)\frac{\partial^2 p}{\partial x^2}. \tag{94}$$

Using eqs (91) and (94), eq. (93) becomes

$$\frac{\partial \eta}{\partial t} = -\left(\frac{4+\alpha_p\sigma_p}{12(1+\alpha_p\sigma_p)}\right)\left[(1 \pm We)\frac{\partial^2 \eta}{\partial x^2} + \frac{1}{B}\frac{\partial^4 \eta}{\partial x^4}\right]. \tag{95}$$

To investigate the growth rate, n of the periodic perturbation of the interface, following the procedure in obtaining eq. (18) from eq. (95) we get

$$n = \left(\frac{4+\alpha_p\sigma_p}{12(1+\alpha_p\sigma_p)}\right)\ell^2\left[(1 \pm We) - \frac{\ell^2}{B}\right]. \tag{96}$$

The Bond number B measures the relative importance of gravitational effect to surface tension and We physically represents the measure of electric energy to pressure energy. In the absence of electric field and porous lining, that is $We \to 0$ and $\sigma_p \to 0$, the growth rate given by eq. (96) reduces to n_b given in the earlier sections. Accordingly, eq. (96) can be written as

$$n = n_b - \frac{\alpha_p\sigma_p}{4(\alpha_p\sigma_p+1)}\ell^2\left(1-\frac{\ell^2}{B}\right) \pm \left(\frac{\alpha_p\sigma_p+4}{\alpha_p\sigma_p+1}\right)\frac{\ell^2}{B}We. \tag{97}$$

The positive or negative sign in the third term in eq. (97) will depend, as stated earlier, on whether the potential difference is along or opposing the gravity. In our configuration the lower plate is maintained at a higher potential than at the upper plate. That is, the potential differences opposes gravity and hence we have to choose the negative sign in eq. (97), and obtain a dispersion formula of the form

$$n = n_b - \ell\beta v_a, \tag{98}$$

where

$$\beta = \frac{3\alpha_p\sigma_p\left(1-\frac{\ell^2}{B}\right) - We(4+\alpha_p\sigma_p)}{(4+\alpha_p\sigma_p)\left(1-\frac{\ell^2}{B}-We\right)}$$

and

$$v_a = \frac{(4+\alpha_p\sigma_p)\ell}{12(1+\alpha_p\sigma_p)}\left(1-\frac{\ell^2}{B}-We\right).$$

The expressions are computed and the results are discussed in the final section.

Conclusion

Linear and nonlinear RTI have been discussed in this article. The linear RTI in a thin film-shell lined with an incompressible fluid-saturated porous lining with uniform densities has been investigated using normal mode analysis. The dispersion relations are given by eqs (18), (42), (62) and (97) and they are analogous to those given by Takabe *et al.*[12] as shown in eq. (4). The dispersion relation (17) coincides with one given by Babchin *et al.*[5] in the absence of porous lining (i.e. $\sigma \to 0$).

Setting $n = 0$ in dispersion relations mentioned above, we get the cut-off wavenumber ℓ_{cl} above which RT instability is stabilized. Setting $\partial n/\partial \ell = 0$, we obtain the maximum wavenumber, ℓ_m. Substituting this ℓ_m in the dispersions relations we get the maximum growth rate n_m. As a sample, this procedure is illustrated by considering Problem 1. The same procedure can be applied to other problems as discussed in the article.

Setting $n = 0$ in dispersion relation, eq. (16) we get the cut-off wavenumber

$$\ell_{ct} = \sqrt{B/2}, \tag{99}$$

because α, σ and ℓ are different from zero. The maximum wavenumber ℓ_m, obtained from eq. (18) by setting $\partial n/\partial \ell = 0$, is

$$\ell_m = \ell_{ct}/\sqrt{2}. \tag{100}$$

Equations (99) and (100) are true even for the case in the absence of porous lining obtained from eq. (17), and for convenience we call them as classical results. The corresponding maximum growth rate, n_m is

$$n_m = \frac{B}{48}\frac{(4+\alpha\sigma)}{(1+\alpha\sigma)}, \quad n_{bm} = \frac{B}{12}, \quad \frac{n_m}{n_{bm}} = \frac{(4+\alpha\sigma)}{4(1+\alpha\sigma)}. \tag{101a–c}$$

It will be of interest to compare these results with those given in eq. (4) by Takabe *et al.*[12]. In their case

$$(\ell_{ct})_{T_a} = \frac{0.81g}{\beta^2 v_a^2} \quad \text{and} \quad (\ell_m)_{T_a} = \frac{0.81g}{4\beta^2 v_a^2} = \frac{(\ell_{ct})_{T_a}}{4}. \tag{102}$$

The corresponding n_m is

$$(n_m)_{T_a} = 0.45\sqrt{(\ell_m)_{T_a} g} = 0.45(n_b)_{T_a}, \tag{103}$$

where the quantities with suffix T_a correspond to those given by Takabe *et al.*[12]. They have shown that the maxi-

mum ratio of growth rate was reduced to 45% of their classical value $(n_b)_{T_a}$, using eq. (103). However, the reduction of maximum ratio of growth rate in the case of porous lining given by eq. (101c) depends on α and σ of the porous lining. For the type of porous material used in the experiments of Beavers and Joseph[4], α ranges from 0.1 to 4.0 and σ ranges from 4 to 20. Then, for $\alpha = 0.1$ and $\sigma = 4$, the maximum ratio of growth rate, G_m given in Table 2 is reduced to 78.57% of the classical value n_{mb}, whereas for $\alpha = 0.1$ and $\sigma = 20$, the maximum growth rate is reduced to 50% of the classical value. Similarly, for $\alpha = 4.0$ and $\sigma = 4$, n_m is reduced to 29.41% of n_{bm}, whereas for $\alpha = 4.0$ and $\sigma = 20$, n_m is reduced to 26.15% of n_{bm}.

From these, we conclude that a simple model of incompressible homogenous fluid, with a proper choice of material (i.e. α and σ) for porous lining, reduces the growth rate of RTI mode even up to 80% compared to the classical value without porous lining. This is a considerable reduction in the ratio of growth rate compared to that achieved by Takabe *et al.*[12] without porous lining. This conclusion on the reduction of growth rate of RTI mode is useful in the design of suitable pellets for effective extraction of IFE. This mechanism is also useful in some biomechanical problems like coronary artery diseases, where plaques are formed on the endothelium (i.e. walls of the arties) due to accumulation of cholesterol and other fatty substances which cause a constriction called stenosis. Nowadays, instead of bypass surgery, like laser surgery is used to dissolve the plaques. This has a side effect, for example, eroding the endothelium. To overcome this, it is advantageous to have nanostructure porous lining. The porous lining is essential to transport nutrients from the arteries needed for the body.

The nonlinear problem discussed earlier is quite different from that of Babchin *et al.*[5], considering plane Couette flow. The present problem is influenced by the slip velocity at the interface between the porous layer and thin film. It is not amenable to analytical treatment as in the case of Babchin *et al.*[5]. Therefore, numerical solutions are obtained using fourth-order accurate central differences for spatial discretization. For large porous parameters of the order of $\sigma = 10^4$, however, it was not possible to obtain smooth solutions. Instead, chaotic but bounded solutions appeared which could not be avoided by increasing the number of grid points dramatically. A remedy might be to use upwind discretizations or to add artificial viscosity terms to the centrally discretized terms.

From the two-dimensional RTI investigation we can conclude that eq. (35) is in agreement with the results of Brown[26]. As in the case of Brown, we found that even in the case of finite thickness film bounded on one side by a porous layer, the size scale of RTI was controlled by the ratio of surface tension to the density gradient when the film was thin.

Effects of laser radiation and porous lining on the growth rate have been determined, and computed for different values of the Bond number B and temperature difference $\theta_p - \theta_f$. The results are depicted in Figure 4 *a–c*. From these we conclude that the nature of the dispersion curve is influenced by both the difference in temperature, namely $\theta_p - \theta_f$, and the bond number B. From Figure 4 it is clear that the growth rate decreases with a decrease in B, implying increase in surface tension, and an increase in $\theta_{p_1} - \theta_{f_1}$ increases the growth rate. That is, increase in surface tension makes the interface more stable and increase in $\theta_{p_1} - \theta_{f_1}$ makes the interface more unstable.

Expressions for ℓ_{ct}, ℓ_m, n_m, n_{bm} and $G_m = n_m/n_{bm}$ have been obtained. We note that since n_m and n_{bm} are both proportional to $(\theta_p - \theta_f)^2$, they disappear from G_m. These are computed and the results are given in Table 2.

From Table 2, it is clear that an increase in α as well as σ decreases G_m considerably. It is clear that when $\sigma = 4$ and $\alpha = 0.1$, ratio of growth rate decreases about 79% compared to the classical growth rate, which is favourable for efficient extraction of IFE.

The temperature distribution given by eq. (48) is computed for different values of buoyancy parameter N and the results are graphically represented in Figure 6. From Figure 6 it is clear that for small values of $N \leq 0.1$, the temperature is parabolic in nature, while for curves of $N \geq 0.1$, the temperature decreases and almost becomes a straight line. That is, large values of N flatten the temperature profile.

The value of θ_B given by eq. (51) is computed for different values α, σ and N, and the results are graphically represented in Figure 7 *a–c*. From Figure 7, we conclude that θ_B increases with an increase in α. It is clear that for

Table 2. The ratio of maximum growth rate

	G_m		
σ	$\alpha = 0.1$	$\alpha = 4.0$	$\alpha = 12.0$
4	0.7857	0.2941	0.2653
20	0.5000	0.2593	0.2531
30	0.4375	0.2562	0.2521

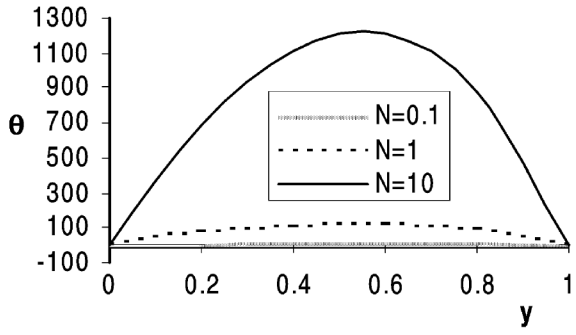

Figure 6. Temperature distribution vs y for different values of N.

values of $\sigma < 10$, θ_B increases slowly and saturates for larger values of $\sigma > 10$. The temperature gradient at the wall $y = 1$ is computed for different values of N and the results are given in Table 3. Form Table 3 it is clear that an increase in N increases the temperature gradient and is hence favourable for heat transfer.

The linear RTI in an IFE target modelled as a thin electrically conducting fluid-film in the presence of transverse magnetic field lined with an incompressible electrically conducting fluid-saturated porous lining with uniform densities has been investigated using normal mode analysis. The main objective of this study is to show that the two mechanisms, i.e. having a suitable strength of magnetic filed and suitable porous material, reduce the growth rate of ablative surface of IFE target considerably compared to that in their absence. The dispersion relations given by eqs (62)–(66a–c) are analogous to those given by Takabe *et al.*[12] for non-electrically conducting fluid. The dispersion relation given by eq. (65) coincides with the one given by Babchin *et al.*[5] in the absence of both magnetic field ($M \to 0$) and the nanostructure porous lining ($\sigma \to 0$).

In the presence of magnetic field and absence of porous lining ($\sigma = 0$, $\alpha = 0$), it is clear that the maximum growth rate n_m depends on the Hartman number M. We note that G_m purely depends on porous lining when $M = 0$, and generally depends on M, α and σ.

The expressions for ℓ_{ct}, ℓ_m, n_m, n_{bm} and $G_m = n_m/n_{bm}$ are obtained and numerically computed for different values of M (0.1, 1, 10, 100), σ (0, 4, 10, 20) and α (0.1, 4). From this it is clear that the percentage of decrease in ratio of growth rate compared to the classical growth is maximum, for example 99.99 for small values of M, say 0.1 and decreases for large values of M. The same behaviour is true for increase in σ and α.

Equation (62) is plotted in Figure 8, for the growth rate n vs wavenumber ℓ for $M = 1$, $\alpha = 0.1$ and $\sigma = 4$, and for different values of B. From Figure 8 we conclude that the perturbation of the interface having a wavenumber smaller than ℓ_{ct} is amplified when $\delta > 0$ (i.e. $\rho_f < \rho_p$) and the growth rate decreases with decrease in B, implying increase in surface tension. That is, increase in surface tension makes the interface more stable even in the case of electrically conducting fluid. Similar behaviour is observed for $M > 1$ for fixed values of α and σ. Increase in σ is more significant than increase in M in reducing the ratio of growth rate.

The ablative temperature θ_B given by eq. (71) is computed for different values of M, σ and for fixed values of α (Tables 4 and 5). The results of θ_B vs M for different

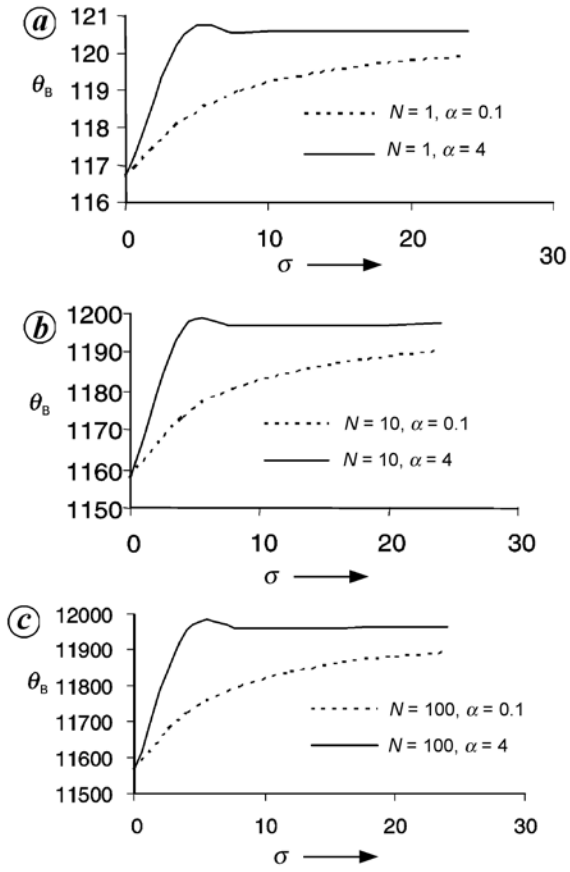

Figure 7 *a–c*. Ablative surface temperature θ_B.

Table 3. Temperature gradients

N	$-\left(\frac{\partial\theta}{\partial y}\right)_{y=1}$ from eq. (49)	$-\left(\frac{\partial\theta}{\partial y}\right)_{y=1} \times 10^{-3}$ from eq. (49)
1	0.3649	0.3193
10	2.7917	3.1935
100	27.0594	31.9350
1000	269.737	319.350

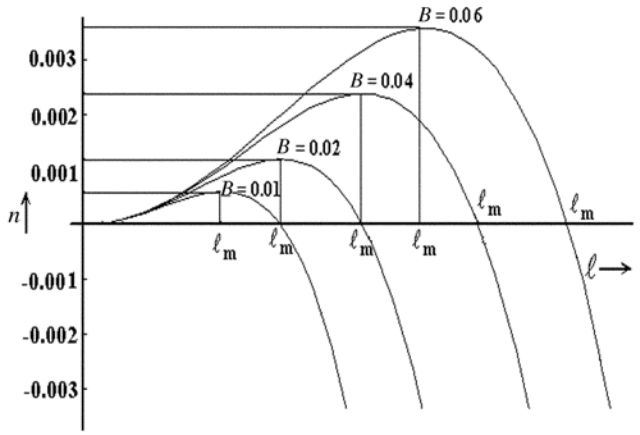

Figure 8. Growth rate n vs wavenumber ℓ for $M = 1$ and for different Bond numbers B.

values of σ are plotted in Figure 9, and θ_B vs σ for different values of M are plotted in Figure 10. We conclude that for small values of M and σ, θ_B increases slowly, and saturates for larger values of M and σ.

The effect of transverse electric field and nanostructured porous lining on the linear ERTI in a thin shell filled with incompressible, poorly conducting fluid has been studied using normal mode analysis. The analytical simple formula for dispersion relation, eq. (97) is analogous to the one given by Takabe *et al.*[12] for compression of fluid by laser, and is analogous to the one given by Rudraiah[3] for incompressible fluid with nanostructured porous lining and in the absence of electric field. The dispersion relation n_b given in eq. (98) coincides with the one given by Rudraiah[3] in the absence of electric field. The expression for ℓ_{ct}, ℓ_m, n_m, n_{bm} and G_m are obtained. They are computed for different values of We, α and σ, and percentage of decrease in the ratio of growth rate compared to classical growth rate is given in Table 6.

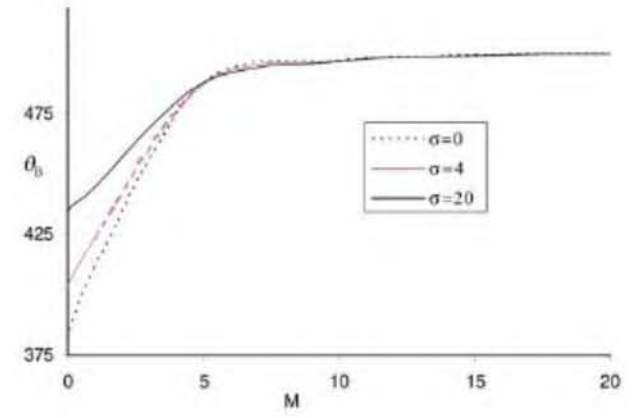

Figure 9. Ablative surface temperature θ_B for different σ.

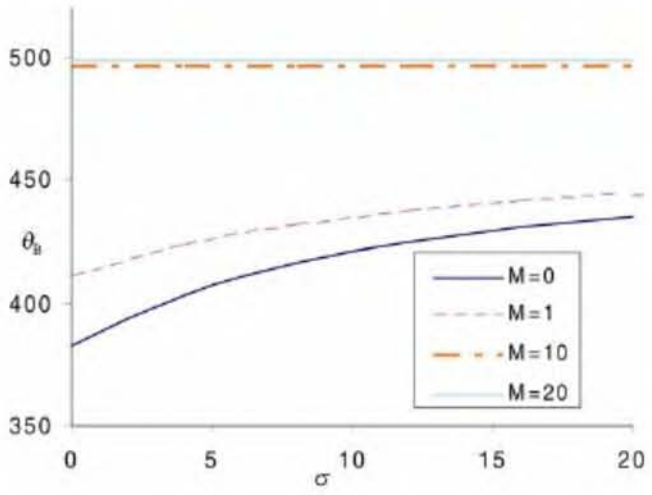

Figure 10. Ablative surface temperature θ_B for different M.

We note that in the case of applied voltage opposing gravity $\ell_{ct} = \sqrt{B(1-We)}$ and $\ell_m = \ell_{ct}/\sqrt{2}$ are real only if $We \leq 1$. However, in the case of applied voltage in the direction of gravity, $\ell_{ct} = \sqrt{B(1+We)}$ and $\ell_m = \ell_{ct}/\sqrt{2}$. Here, we get $(1 + We)$ and hence in that situation ℓ_{ct} and ℓ_m are real for all values of We.

The corresponding maximum growth rate, n_m for applied voltage opposing gravity is

$$n_m = \frac{B}{48}\left(\frac{\alpha_p\sigma_p + 4}{\alpha_p\sigma_p + 1}\right)(1-We)^2. \tag{104}$$

n_m will be zero for $We = 1$. Physically this implies the equi-partition of energy (i.e. electric energy balances pressure energy). Since pressure has the dimension of kinetic energy, this equi-partition can also be stated as electric energy balances kinetic energy. If we choose the voltage such that $We = 1$, asymmetry can be completely reduced and hence maximum efficiency of IFE may be achieved. Since $\ell_m = \sqrt{B/2}$, $n_{bm} = B/12$, then $G_m = n_m/n_{bm}$ is

$$G_m = \left(\frac{\alpha_p\sigma_p + 4}{4(\alpha_p\sigma_p + 1)}\right)(1-We)^2. \tag{105}$$

G_m is computed for different values of α_p, σ_p and We (Table 6). From Table 6 it is clear that nanostructured porous lining and external constraint of electric field are more effective than the effect of compression due to laser in reducing the growth rate of RTI. In particular for $We = 1$, complete symmetry can be maintained because $n_m = 0$ and hence $G_m = 0$ for $We = 1$.

The growth rate n given by eq. (96) takes the form

$$n = \frac{4+\alpha_p\sigma_p}{12(\alpha_p\sigma_p + 1)}\ell^2\left[(1-We) - \frac{\ell^2}{B}\right]. \tag{106}$$

Table 4. The values of θ_B for different σ

σ	$M = 0$	$M = 1$	$M = 10$	$M = 20$
0	382.264	410.918	496.739	498.861
4	403.504	423.383	496.756	498.865
8	416.156	431.443	496.772	498.868
12	424.549	437.081	496.786	498.871
16	430.523	441.247	496.799	498.874
20	434.991	444.45	496.812	498.876

Table 5. The values of θ_B for different M

M	$\sigma = 0$	$\sigma = 4$	$\sigma = 20$
0	382.3	403.5	434.99
1	410.9	423.4	444.5
5	486.9	487.1	487.5
10	496.7	496.8	496.8
15	498.86	498.86	498.88
20	499.64	499.64	499.65

Table 6. Comparison of results

Authors	G_m	Percentage of reduction in the ratio of growth rate
Takabe *et al.*[12]	0.45	45 (for compressible fluid)
Present study – Problems 1 and 4	0.79	79 ($\alpha_p = 0.1$, $\sigma_p = 4$)
Present study – Problem 5 for $\alpha = 0$, $\sigma = 0$	0.99996	(for incompressible fluid)
	0.7152	99.99 for $M = 10^{-1}$
	0.0027	71.52 for $M = 10^{0}$
	0.0003	2.7 for $M = 10^{1}$
		0.03 for $M = 10^{2}$ (for MHD)
Present study – Problem 5 for $\alpha = 0.1$, $\sigma = 4$	0.7296	73 ($\alpha_p = 0.1$, $\sigma_p = 4$, $M = 0.5$)
	0.59	59 ($\alpha_p = 0.1$, $\sigma_p = 10$, $M = 0.5$)
	0.48	48 ($\alpha_p = 0.1$, $\sigma_p = 20$, $M = 0.5$)
	0.29	29 ($\alpha_p = 4.0$, $\sigma_p = 4$, $M = 0.5$)
	0.60	60 ($\alpha_p = 0.1$, $\sigma_p = 4$, $M = 1$)
	0.50	50 ($\alpha_p = 0.1$, $\sigma_p = 10$, $M = 1$)
	0.42	42 ($\alpha_p = 0.1$, $\sigma_p = 20$, $M = 1$)
	0.26	26 ($\alpha_p = 4.0$, $\sigma_p = 4$, $M = 1$)
Present study – Dispersion relation for $\alpha = 0$, $\sigma = 0$	0.98	98 for $We = 10^{-2}$
	0.81	81 for $We = 10^{-1}$
Present study – Dispersion relation for different values of We for fixed α_p, σ_p	0.64	64 ($\alpha_p = 0.1$, $\sigma_p = 4$, $We = 0.1$)
	0.442	44.2 ($\alpha_p = 0.1$, $\sigma_p = 4$, $We = 0.25$)
	0.1964	20 ($\alpha_p = 0.1$, $\sigma_p = 4$, $We = 0.5$)
	0.0491	0.5 ($\alpha_p = 0.1$, $\sigma_p = 4$, $We = 0.75$)
	0	0 ($\alpha_p = 0.1$, $\sigma_p = 4$, $We = 1.0$)

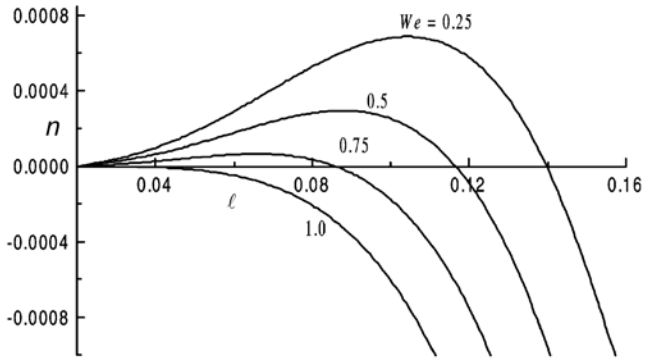

Figure 11. Growth rate n vs wavenumber ℓ for different values of electric parameter We, when $\alpha_p = 0.1$, $\sigma_p = 4$ and $B = 0.02$.

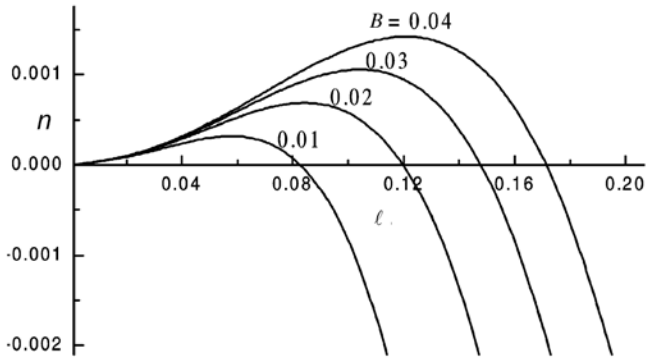

Figure 12. Growth rate n vs wavenumber ℓ for different values of Bond number B, when $\alpha_p = 0.1$, $\sigma_p = 4$ and $We = 0.25$.

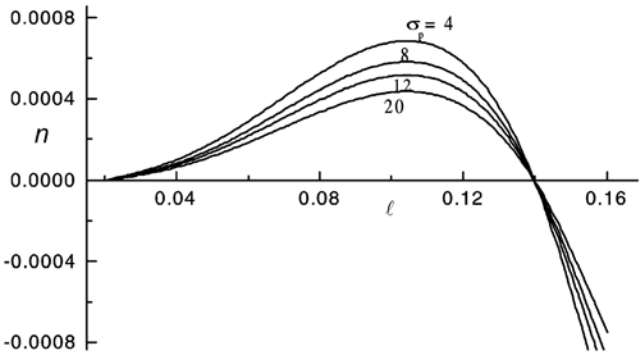

Figure 13. Growth rate n vs wavenumber ℓ for different values of porous parameter σ_p, when $\alpha_p = 0.1$, $B = 0.02$ and $We = 0.25$.

If $1 - We = \ell^2/B$, then $n = 0$ and hence the interface is neutrally stable. If $We < 1 - \ell^2/B$, then $n > 0$ and hence the surface is unstable. If $We > 1 - \ell^2/B$, then $n < 0$ and hence the surface is stable. From this we conclude that by suitably selecting the values of We it is possible to control a growth rate. The growth rate n given by eq. (106) is numerically computed for different values of We, B and σ_p, and the results are given in Figure 11 for n vs ℓ for different values of We. From Figure 11 it is clear that the decrease in growth rate compared to the classical growth rate is steep for We in the range 0.5–1.0. Equation (106) is plotted in Figure 12 for growth rate n vs the wavenumber ℓ for $We = 0.25$ and for different values of the Bond number B. From Figure 12, it is clear that the perturba-

tions of the interface having ℓ smaller than the ℓ_{ct} are amplified when $\delta > 0$ (i.e. $\rho_f < \rho_p$) and the growth rate decreases with a decrease in B, implying increase in surface tension because B is the reciprocal of surface tension. From this it is clear that an increase in surface tension decreases the growth rate and hence makes the interface more stable. Also, eq. (106) is plotted in Figure 13 for the growth rate n vs the wavenumber ℓ for different values of porous parameter σ_p for fixed α_p, B and We. From Figure 13 we conclude that the decrease in the growth rate is steep compared to the classical growth rate for different values σ_p in the range 4–20.

1. Hogan, W. J. and Bertel, E., *Energy from Inertial Fusion*, IAEA, Vienna, 1995, vol. 1, pp. 1–11.
2. Rudraiah, N., Krishnamurthy, B. S., Jalaja, A. S. and Desai, T., Effect of a magnetic field on the growth rate of Rayleigh–Taylor instability of a laser accelerated thin ablative surface. *Laser Part. Beam*, 2004, **22**, 1–5.
3. Rudraiah, N., Effect of porous lining on reducing the growth rate of Rayleigh–Taylor instability in the inertial fusion energy target. *Fusion Sci. Technol.*, 2003, **43**, 1–5.
4. Beavers, G. S. and Joseph, D. D., Boundary conditions at a naturally permeable wall. *J. Fluid Mech.*, 1967, **30**, 197–207.
5. Babchin, A. J., Frenkel, A. L., Levich, B. G. and Shivashinsky, G. I., Nonlinear saturation of Rayleigh–Taylor instability in thin films. *Phys. Fluids*, 1983, **26**, 3159–3161.
6. McCrory, R. L., Montierth, L., Morse, R. L. and Verdon, C. P., Nonlinear evolution of ablation-driven Rayleigh–Taylor instability. *Phys. Rev. Lett.*, 1981, **46**, 336–339.
7. Nakai, S. and Takabe, H., Principles of inertial confinement fusion–Physics of implosion and the concept of inertial fusion energy. *Rep. Prog. Phys.*, 1996, **59**, 1071–1131.
8. Desai, T. and Pant, H. C., Control of Rayleigh–Taylor instabilities in laser accelerated seeded target. *Laser Part. Beam*, 2000, **18**, 119–128.
9. Borisenko, N. G. and Merkuiev, Y. A., Physics Institute, Moscow, 1990, Preprint 47.
10. Mikaelian, K. O., Effect of viscosity on Rayleigh–Taylor and Richtmyer–Meshkov instabilities. *Phys. Rev. E*, 1993, **47**, 375–385.
11. Rudraiah, N., Krishnamurthy, B. S. and Mathad, R. D., The effect of oblique magnetic field on the surface instability of a finite conducting fluid layer. *Acta Mech.*, 1996, **119**, 165–180.
12. Takabe, H., Mima, K., Montierth, L. and Morse, R. L., Self-consistent growth rate of the Rayleigh–Taylor instability in an ablatively accelerating plasma. *Phys. Fluids*, 1985, **28**, 3676–3682.
13. Bernstein, I. B. and Book, D. L., Effect of compressibility on the Rayleigh–Taylor instability. *Phys. Fluids*, 1983, **26**, 453–458.
14. Sethian, J. D. *et al.*, Direct drive acceleration of planar liquid deuterium targets. *Phys. Plasma*, 1999, **6**, 2089–2094.
15. Batani, D., Nazaroy, W., Koenig, M. and Hall, T., *Recent Res. Dev., Plasma*, 2000, **1**, 65–88.
16. Carles, P., Huang, Z., Carbone, G. and Rosenblatt, C., Rayleigh–Taylor instability for immiscible fluids of arbitrary viscosities: A magnetic levitation investigation and theoretical model. *Phys. Rev. Lett.*, 2006, **96**, 104501.
17. Rudraiah, N., *Nonlinear Fluid through Porous Media in Nonlinear Phenomena* (eds Malik, S. K. *et al.*), Indian National Science Academy, New Delhi, 2000, pp. 601–681.
18. Kull, H. J., Theory of Rayleigh–Taylor instability. *Phys. Rep.*, 1991, **206**, 198–325.
19. Rudraiah, N., Mathad, R. D. and Betigeri, H., The RTI of a viscous fluid layer with viscosity stratification. *Curr. Sci.*, 1997, **72**, 391–395.
20. Saffman, P. G., On the boundary condition at the surface of a porous medium. *Stud. Appl. Math.*, 1971, **50**, 93–101.
21. Yiantsios, S. G. and Higgins, B. G., Rayleigh–Taylor instability in thin viscous films. *Phys. Fluids A1*, 1984.
22. Rudraiah, N. and Ng, C. O., A model for manufacture of nanostructure of nanosized smart material free from impurities. *Curr. Sci.*, 2004, **86**, 1076–1091.
23. Chapra, S. C. and Canale, R. P., *Numerical Methods for Engineers*, McGraw, New York, 1998, 2nd edn.
24. Rudraiah, N., Wagner, G. S., Evans, G. S. and Friedrich, R., Nonlinear study of Rayleigh–Taylor Instability in thin films past a porous layer. *Indian J. Pure Appl. Math.*, 1998, **29**, 417–431.
25. Rudraiah, N., Shivakumara, I. S. and Chavaraddi, K. B., Electrohydrodynamic Rayleigh–Taylor instability with finite thickness porous lining of smart material of nanostructure at the ablative surface. *Int. J. Fluid Mech. Res.*, 2007 (in press).
26. Brown, H. R., Rayleigh–Taylor instability in a finite thickness layer of a viscous fluid. *Phys. Fluids A*, 1989, **50**, 895–896.
27. Lindl, J. D., Development of the indirect-drives approach to inertial confinement fusion and target physics basis for ignition. *Phys. Plasma*, 1995, **2**, 3933–3941.
28. Betti, R., Gonharov, V. N., McCrory, R. L. and Verdon, C. P., Self-consistent cut-off wave number of the ablative Rayliegh–Taylor instability. *Phys. Plasma*, 1985, **2**, 3844.
29. Kilkenney, J. D. *et al.*, A review of the ablative stabilization of the Rayleigh–Taylor instability in regimes relevant to inertial confinement. *Phys. Plasma*, 1994, **1**, 1379–1386.
30. Kanuer, J. P. *et al.*, Single-mode, Rayleigh–Taylor growth rate measurements on the OMEGA laser system. *Phys. Fluids*, 2002, **7**, 338–345.
31. Rudraiah, N., Shivakumara, I. S. and Chavaraddi, K. B., Electrohydrodynamic Rayleigh–Taylor instability in a finite thickness layer of poorly conducting viscous fluid. In Proceedings of the International Symposium on Recent Advances in Fluid Mechanics, Bangalore University, 2004, pp. 305–314.

ACKNOWLEDGEMENTS. N.R. is grateful to Prof. M. Kalal, Czech Technical University, Prague for inviting him and also acknowledges ISRO for financial support under Respond project 2007.

Received 18 January 2007; revised accepted 3 August 2007